공학박사 학위논문

BIO-POLYMERIC DRUG-DELIVERY STRAND FOR MEDICAL DEVICE APPLICATION

의료기기 적용을 위한 약물전달 기능 생체 고분자 스트랜드

2019 년 2 월

서울대학교 대학원

협동과정 바이오엔지니어링 전공

허 범 강

BIO-POLYMERIC DRUG-DELIVERY STRAND FOR MEDICAL DEVICE APPLICATION

의료기기 적용을 위한 약물전달 기능 생체 고분자 스트랜드

지도 교수 최 영 빈

이 논문을 공학박사 학위논문으로 제출함

2019 년 2 월

서울대학교 대학원

협동과정 바이오엔지니어링 전공

허 범 강

허범강의 공학박사 학위논문을 인준함

2019 년 2 월

위 원 장 최 진 욱 (인)

부위원장 최 영 빈 (인)

위 원 이 정 찬 (인)

위 원 정 기 훈 (인)

위 원 박 한 수 (인)

Ph. D. Dissertation

BIO-POLYMERIC DRUG-DELIVERY STRAND FOR MEDICAL DEVICE APPLICATION

BY

BEOM KANG HUH

FEBRUARY 2019

INTERDISCIPLINARY PROGRAM IN BIOENGINEERING

THE GRADUATE SCHOOL

SEOUL NATIONAL UNIVERSITY

BIO-POLYMERIC DRUG-DELIVERY STRAND FOR MEDICAL DEVICE APPLICATION

BY

BEOM KANG HUH

INTERDISCIPLINARY PROGRAM IN BIOENGINEERING

THE GRADUATE SCHOOL

SEOUL NATIONAL UNIVERSITY

THIS DISSERTATION IS APPROVED FOR THE DEGREE OF DOCTOR OF PHILOSOPHY

FEBRUARY 2019

DOCTORAL COMMITTEE:

Chairman	*Jinwook Choi, Ph. D.*
Vice Chairman	*Young Bin Choy, Ph. D.*
Member	*Jung Chan Lee, Ph. D.*
Member	*Keehoon Jung, Ph. D.*
Member	*Hansoo Park, Ph.D.*

Abstract

BIO-POLYMERIC DRUG-DELIVERY STRAND FOR MEDICAL DEVICE APPLICATION

By

Beom Kang Huh

Interdisciplinary Program in Bioengineering

The Graduate School

Seoul National University

The present thesis focuses on the design, fabrication and evaluation of strand-based drug delivery medical devices that can support the function of implantable medical devices. In order to ensure biocompatibility of strand-based drug delivery medical devices post-implantation, the strands were prepared using the electrospinning and electro-spraying methods using a bio-polymer.

In recent years, numerous medical devices have been developed to diagnose, cure, treat, and prevent diseases in humans

and other animals. However, the materials used in manufacturing these medical devices are foreign substances to the body and, therefore, can cause pain, abnormal fibrosis, as well as capsular contracture from inflammation. The approaches commonly used to solve these issues include oral drug administration and drug injection; however, these approaches may also cause secondary side effects such as hepatotoxicity or additional pain. Despite advances in recent research on local drug delivery systems of medical devices where a considerable reduction of these side effects was reported, there are still limitations such as difficulty of transferring the controlled amount of drugs or the reduction in devices' functionality.

In order to solve the aforementioned problems, in the present study, I developed the individual drug delivery carrier based on strands. This carrier releases an appropriate amount of drugs to a local area without compromising the functionality of the device.

In the first experiment, a new drug delivery medical device containing a strand-based controllable drug delivery system was developed. The developed drug delivery strand can maintain the original functionality of the suture and mitigate the pain arising from inflammation. This strand, manufactured using the electro-spraying method, was cut into 1.5 mm in width and then was physically braided to the suture. As shown by the results, the drug delivery strand braided suture was able to maintain the mechanical strength of the suture and consistently released drugs for 10 days while simultaneously suppressing pain arising from inflammation.

In the second experiment, with the aim of reducing the inflammation caused by silicone implants, I fabricated an elastic net that had a controlled drug delivery system. This elastic net was fabricated by 4 strands of 3 mm in width. At this time, the strands were electrospun with mixture of polyurethane and a steroidal drug. It is widely known that inflammation from the insertion of silicone implants can cause abnormal fibrosis, which then leads to the creation of a capsular contracture. This capsular contracture can not only induce pain in, but also result in the need for an additional surgery. However, as shown by the results of the second experiment, the manufactured elastic net suppressed inflammation, abnormal fibrosis, and the development of a capsular contracture. Furthermore, due to its elastic material properties, it was also able to cover implants of various sizes.

These strand-based drug delivery carriers have individual properties, such as controllable drug delivery and elasticity. Since each strand can apply to commercialized medical device, the device can maintain its own functionality in the human body, but also has an additional function to resolve the adverse effects or limitations of drug delivery system. Therefore, these strand-based drug delivery carriers have proven to be effective medical devices that can accurately control and deliver drugs while maintaining full functionality of the original medical device.

Keywords : inflammation, controllable drug delivery, strand, bio-polymer, medical device

Student Number : 2013-31001

Contents

Abstract i

Contents v

List of Tables viii

List of Figures ix

Chapter 1. Introduction 1

1.1 Medical Devices and Inflammation 1

1.2 Previous Approaches of Local Drug Delivery in Medical Devices 4

1.3 Research Aims 11

Chapter 2. Surgical Suture Braided with a Diclofenac-loaded Strand for Local, Sustained Pain Mitigation 15

2.1 Introduction 15

2.2 Materials and Methods 19

2.2.1 Materials 19

2.2.2 Fabrication of Drug-delivery Strands and Sutures 20

2.2.3 Characterization Methods 22

2.2.4 *In vitro* Drug-release Study 23

2.2.5 *In vivo* Pain-relief Evaluation 24

2.2.6 Histological Evaluation 25

2.2.7 Statistical Analysis 26

2.3 Results and Discussion 27
2.3.1 Chracterization of Strands and Sutures 27
2.3.2 *In vivo* Efficacy Evaluation 37
2.3.3 Histological Evaluation 41
2.4 Conclusion 44

Chapter 3. Elastic Net of Polyurethane Strand for Sustained Release of Triamcinolone Around Silicone Implant of Various Sizes 45

3.1 Introduction 46
3.2 Materials and Methods 49
3.2.1 Materials 49
3.2.2 Preparation of Silicone Samples and DDN 50
3.2.3 Characterization 53
3.2.4 *In vitro* Drug Release Study 54
3.2.5 *In vivo* Experiments 54
3.2.6 Histological and Immunofluorescence Analysis 55
3.2.7 Statistical Analysis 57
3.3 Results 59
3.3.1 Strand Characterization 59
3.3.2 *In vitro* Release Profiles of triamcinolone 62
3.3.3 *In vivo* Evaluation 64
3.4 Discussion 97
3.4 Conclusion 98

Chapter 4. Conclusion and perspectives 99

References 103

Abstract in Korean 112

Acknowledgement 115

List of Tables

Table 2.1 Mechanical properties of the sutures 35

List of Figures

Figure 1.1 Commercialized antibacterial suture by Ethicon 9

Figure 1.2 Schematic drawing of the surgical procedure. The needle tip inserted into a capsule of the implant under ultrasound guidance. Dotted line = contracted capsule 10

Figure 2.1 Schematic showing the process of preparing the drug-delivery suture 21

Figure 2.2 Fourier transform infrared spectra of intact DF, intact PLGA, PLGA strand and PLGA_DF strand 31

Figure 2.3 X-ray diffraction patterns of intact DF, intact PLGA, PLGA strand and PLGA_DF strand 32

Figure 2.4 Cross-sectional SEM images of (a) original suture, (b) PLGA suture and (c) PLGA_DF suture. The inserts in (b) and (c) show more detailed images of the sutures obtained at larger magnification. The scale bars in the main images and insets are 100 μm and 10 μm, respectively 33

Figure 2.5 Cross-sectional SEM images of (a) PLGA suture and (b) PLGA_DF suture, which are the larger images of the insets in Figure 2.4 (b) and (c), respectively. The scale bars are 10 μm 34

Figure 2.6 *In vitro* drug release profiles of the PLGA_DF suture

.....36

Figure 2.7 Rearing activity obtained in the animal groups; * p<0.05, significantly different from the sham group 39

Figure 2.8 Velocity profiles obtained in the animal groups at 1 day after surgery; * p<0.05, significantly different from the sham group 40

Figure 2.9 Histological analysis of the tissues around the sutures, based on H&E staining. The tissues were biopsied 14 days after surgery. (a) Representative histological images (A: original suture, B: PLGA suture and C: PLGA_DF suture). The scale bars are 100㎛. (b) Inflammation grade scores and (c) inflammatory tissue thicknesses; *<0.05, significantly different from the sham group 42

Figure 3.1 Scanning electron micrographs of the surfaces of the strands for (a) EN_SI, (b) DDN_SI, (c) EN_LI and (d) DDN_LI. Scale bars are 1 ㎛. and optical images of (e) DDN, (f) SI and DDN_SI, and (g) LI and DDN_LI. Scale bars are 1 cm.....52

Figure 3.2 X-ray diffraction patterns of intact triamcinolone, and the strands for EN and DDN.....61

Figure 3.3 *In vitro* cumulative drug release profiles of the DDN_SI and DDN_LI plotted in percent and the amount.....63

Figure 3.4 Evaluation of fibrotic capsules around the silicone implant samples. Profiles of capsule thickness in the

tissues around the silicone implant samples of (a1) small and (b1) large sizes. Asterisk (*) represents a statistically significant difference compared with the intact SI and LI, respectively ($P < 0.01$). Representative H&E-stained images of the tissues around the silicone implant samples of (a2) small and (b2) large sizes obtained at 8 weeks after implantation. Black arrows indicate the capsule thickness. Scale bars are 500 μm. Profiles of collagen density in the tissues around the silicone implant samples of (c1) small and (d1) large sizes. Asterisk (*) represents a statistically significant difference compared with the intact SI and LI, respectively ($P < 0.01$). Representative MT-stained images of the tissues around the silicone implant samples of (c2) small and (d2) large sizes obtained at 8 weeks after implantation. Scale bars are 100 μm....66

Figure 3.5 The capsule thickness around the silicone implants. Representative histological images of (a) SI and (b) LI groups obtained at 2 weeks after implantation. (c) show the comparison of DDN_SI and DDN_LI. The black arrows signify capsule thickness and the scale bars are 500 μm.....71

Figure 3.6 The collagen density around the silicone implants. Representative histological images of (a) SI and (b) LI groups obtained at 2 weeks after implantation. (c) show

the comparison of DDN_SI and DDN_LI. The black arrows signify capsule thickness and the scale bars are 100 μm.....73

Figure 3.7 Profiles of TGF-ß expression in the tissues around the silicone implant samples of (a1) small and (b1) large sizes. Asterisk (*) represents a statistically significant difference compared with the intact SI and LI, respectively ($P < 0.01$). Representative IF-stained images of the tissues around the silicone implant samples of (a2) small and (b2) large sizes obtained at 8 weeks after implantation. White arrow heads indicate the locations of the cells with a double positive signal of green and blue. Scale bars are 100 μm. 75

Figure 3.8 The TGF-β expression in the capsule tissue around the silicone implants. Representative histological images of (a) SI and (b) LI groups obtained at 8 weeks after implantation. (c) show the comparison of DDN_SI and DDN_LI. The scale bars are 100 μm.....78

Figure 3.9 Profiles of fibroblast number in the tissues around the silicone implant samples of (a1) small and (b1) large sizes. Asterisk (*) represents a statistically significant difference compared with the intact SI and LI, respectively ($P < 0.01$). Representative IF-stained images of the tissues around the silicone implant samples of (a2) small and (b2) large sizes obtained at 8

weeks after implantation. White arrow heads indicate the locations of the cells with a double positive signal of green and blue. Scale bars are 100 μm. 80

Figure 3.10 The fibroblast number in the capsule tissue around the silicone implants. Representative histological images of (a) SI and (b) LI groups obtained at 2 weeks after implantation. (c) show the comparison of DDN_SI and DDN_LI. The white arrows signify double signaling of fibroblast and the scale bars are 100 μm. 83

Figure 3.11 Profiles of inflammation degree around the silicone implant samples of (a1) small and (b1) large sizes. Asterisk (*) represents a statistically significant difference compared with the intact SI and LI, respectively ($P < 0.01$). Representative H&E-stained images of the tissues around the silicone implant samples of (a2) small and (b2) large sizes obtained at 2 weeks after implantation. Scale bars are 100 μm 85

Figure 3.12 The degree of inflammation in the capsule tissue around the silicone implants. Representative histological images of (a) SI and (b) LI groups obtained at 8 weeks after implantation. (c) show the comparison of DDN_SI and DDN_LI. The scale bars are 100 μm.....88

Figure 3.13 Side effect evaluation of the silicone implant samples. Profiles of muscle thickness around the silicone implant samples of (a1) small and (b1) large sizes. Asterisk (*)

represents a statistically significant difference compared with the intact SI and LI, respectively ($P < 0.01$). Representative H&E-stained images used for muscle thickness evaluation around the silicone implant samples of (a2) small and (b2) large sizes obtained at 8 weeks after implantation. Black arrows indicate the muscle thickness. Scale bars are 500 μm. Profiles of skin thickness around the silicone implant samples of (c1) small and (d1) large sizes. Asterisk (*) represents a statistically significant difference compared with the intact SI and LI, respectively ($P < 0.01$). Representative H&E-stained images used for skin thickness evaluation around the silicone implant samples of (c2) small and (d2) large sizes obtained at 8 weeks after implantation. Black arrows indicate the skin thickness. Scale bars are 500 μm. 90

Chapter 1

Introduction

1.1 Medical devices and Inflammation

By definition, a medical device is an instrument, implant, machine, or other similar item approved for medical use by US Pharmacopoeia. The intended functions of medical devices include diagnosis, treatment, and prevention of diseases in humans or other

animals (1). Another function of medical devices is helping the body to function properly so that to maintain an appropriate quality of life of patients. Due to the growing demand for medical devices and the functions that they are able to perform, recent years have witnessed a rapid growth and expansion of the medical device market. Various medical devices are still being developed for better disease diagnosis, treatment, and prevention. Overall, medical devices can be broadly categorized into implantable and non-implantable. Devices from the latter group are used on the skin or near the body to monitor or treat various body functions. Relevant examples of non-implantable medical devices include electrocardiography, blood pressure monitors, and defibrillators, all of which have been previously commercialized. By contrast, devices from the former category, i.e. implantable medical devices, are usually used under the skin to replace damaged body functions or to connect organs and tissues. Relevant examples of implantable medical devices are surgical sutures, silicone implants, coronary stents, artificial bones, and heart (2). Of note, while non-implantable medical devices generally have no effect on the human body, implantable medical devices can induce severe side effects (3-5).

One of the most severe side effects induced by implantable medical devices is inflammation (6). Inflammation is a process whereby the body’s white blood cells and substances produced by

those cells protect the body from infection. When medical devices are implanted under the human skin, the foreign body reaction occurs immediately, triggering secretion, by several cytokines and polymorphonuclear leukocytes (i.e., PMNs), of variety of pro-inflammatory cytokines, such as interleukins and tumor necrosis factor-α (TNF-α) (7). As a consequence of the foreign body reaction, inflammation develops around the implanted sites and causes pain, abnormal fibrosis, capsular contractures, and scars (6).

In order to reduce inflammatory reactions triggered by the foreign body reaction, oral drug administration and injection have been widely used. However, despite the seeming ease of these approaches, they also can have secondary side effects. For example, oral drug administration limits drug bioavailability and causes inconveniences to the patients by the requirement of frequent administration. Moreover, this approach may cause toxicity in the gastrointestinal tract or lead to hepatotoxicity (8). With regard to the drug injection approach, it also has its limitations, such as inducing pain in patients. Another limitation of the drug injection approach is that, due to the fast clearance of the drug, it can be difficult to deliver the drug in a sustained manner at the site of action, so multiple treatments will be needed.

In order to reduce the side effects outlined above, more methods to effectively deliver drugs to specific action sites within the

body have been developed. One direction of research has been the development of medical devices that can facilitate a drug's direct reaching the site of action. One a medical device of this type can reach the target site, only a small amount of drug will be needed to do the work, which can effectively reduce adverse side effects associated with the oral drug administration and drug injection methods.

1.2 Previous Approaches of Local Drug Delivery in Medical Devices

As discussed in Section 1.1, due to its convenience, oral drug administration is most commonly used approach to suppress inflammation. However, the limitations of this approach include low drug bioavailability and potentially adverse side effects (9). By contrast, local drug delivery devices can effectively treat diseases while suppressing inflammation and reducing side effects (10).

One type of such local drug delivery devices are surgical sutures. Most surgical sutures are dip-coated in the drug solution to provide the local delivery system. For a better controlled release, drug impregnation, immobilization, and micro-particles are used (11-14). Along with the antibacterial suture that has already been commercialized, many other types of surgical sutures capable of delivering other drugs to reduce side effects have been proposed (see

Figure 1.1).

First of all, there is a large group of surgical sutures for the delivery of various anti-infection drugs. For example, there are sutures coated with biocompatible hydrogel materials that had been immersed into drug solutions, such as tetracyclin, rifampin, or chloramphenicol, for the sustained release (15). In another study, the oxygen plasma treatment was used to impregnate amoxicillin into the suture core so that to considerably enhance the hydrophilicity of muga (*Antheraea assama*) silk fibroin (AASF)-based sutures (16). This suture revealed a clear zone of inhibition against *Escherichia coli (E. coli*) involved in the antibacterial activity. Furthermore, following the commercialization of the Ethicon antibacterial suture in 2004, triclosan-coated surgical sutures have been widely used. The antimicrobial activity of antibacterial surgical suture has been confirmed in many *in vitro* and *in vivo* studies(11, 17-23). A clear zone of inhibition of *E. coli* was exhibited by reducing 96.7 % of bacterial population as compared to the conventional suture, and a better inhibition of bacterial colonization was obtained in the suture implanted site using the mouse and the guinea pig models (17, 18). Besides these dip-coating methods, nanofibers were also used to comprise the body of suture. In one of relevant studies, the electrospinning method was used to fabricate nanofibers by poly (L-lactic acid) (PLLA) and either tetracycline or cefotaxime; afterwards,

the obtained sutures were braided to make a multifilament suture (24, 25). In addition, the coaxial fibers where the drug is located in the middle of each fiber for a better sustained release were also developed. The drug was released more than 10 days, and the antibacterial activity was clearly shown in the clear zone of inhibition against *E.coli.*

Anti-inflammatory surgical sutures were developed by other research groups as well (14, 26-28). For example, sutures were dip-coated with ibuprofen, a nonsteroidal anti-inflammatory drug (NSAID), prepared in the organic solvent dichloromethane (14). As a result, sutures could swell to load a larger amount of the drug into the suture core, which subsequently resulted in a longer (7 days) release period. In another case, sutures were coated with dexamethasone loaded poly (lactic-co-glycolic acid) (PLGA) microparticles (27). In this study, microparticles were coated with polyethyleneimine to have a positive charge which, by electrostatic interactions, could immobilize onto the negatively charged suture surface. As a result, the release period extended to 28 days.

However, despite considerable advances in the development of different drug loading methods, all these methods have several limitations. First of all, mechanical strength of sutures can be affected by an organic solvent that is used. Since many drugs can be dissolved in various organic solvents, the drug coating solution can also dissolve

the suture itself. If this dissolution occurs, the mechanical strength of the suture decreases. Yet, the mechanical strength of a suture is its decisive property as a medical device, as a suture needs to tie the wound or organs. Moreover, given that drugs have different solubility in various solvents, an individual coating procedure may be needed to properly coat the sutures.

As concerns silicone implants, in previous research, inflammation around silicone implant was treated by a local injection of a steroidal drug. As a result, the capsular contracture was successfully reduced when treated with triamcinolone, a steroidal drug (29) (see Figure 1.2). However, effective methods to fabricate a local drug delivery system have not been proposed yet. In the study referred to above, the injected drug cleared out fast, which necessitated the use of additional medication ultrasound guidance to inject drug in the appropriate position. In another study, triamcinolone was spray-coated on the surface of the silicone implant shell to release triamcinolone in a sustained manner (30). Due to the swelling effect of silicone, the drug was deeply diffused and released up to 12 weeks. Inflammation and capsular contracture were reduced *in vivo*. However, considering that the spray condition is fixed, this method is applicable only to a single-sized silicone implant shell. Therefore, it is necessary to develop another process that would make it possible to coat silicone implants of different sizes and to ensure that all them

have the same effect of the spray-coated implant. In clinical settings, since different amounts of drugs are needed to properly suppress inflammation and capsular contracture in the patients of different body proportions, different sizes of silicone implants are needed. Therefore, an additional method for drug loading process that would enable appropriate drug delivery methods has to be developed.

In this context, in order to overcome the limitations outlined above, the present study focused on stand-based carriers that can deliver drugs without changing the functions of medical devices. The carrier developed in the present study can be applied to v implantable medical devices of various sizes. Furthermore, in the proposed carrier, the release of drug can be controlled. Therefore, the carrier developed in the present study can be competitive in many medical device markets.

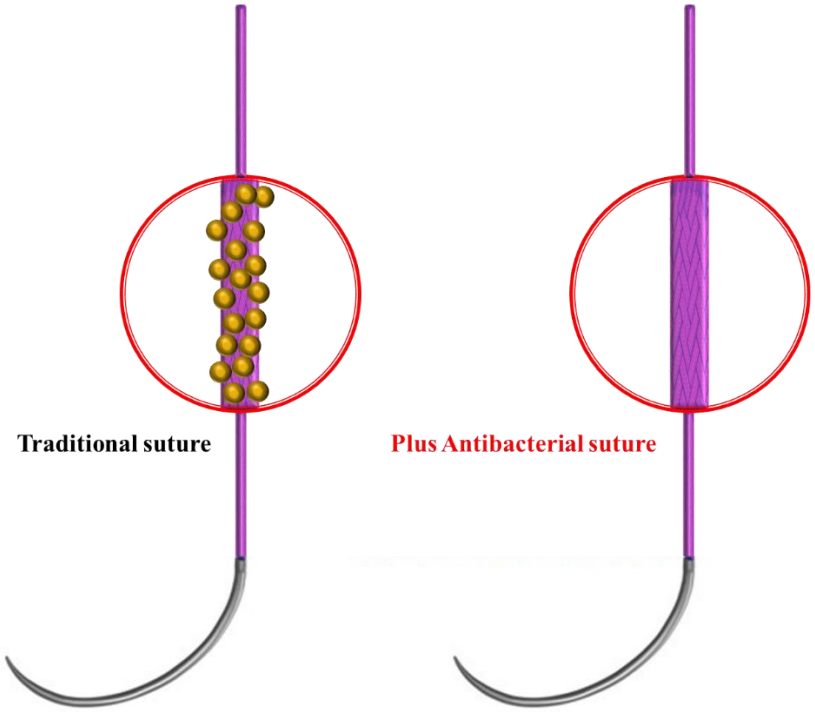

Figure 1.1. Commercialized antibacterial suture by Ethicon (31)

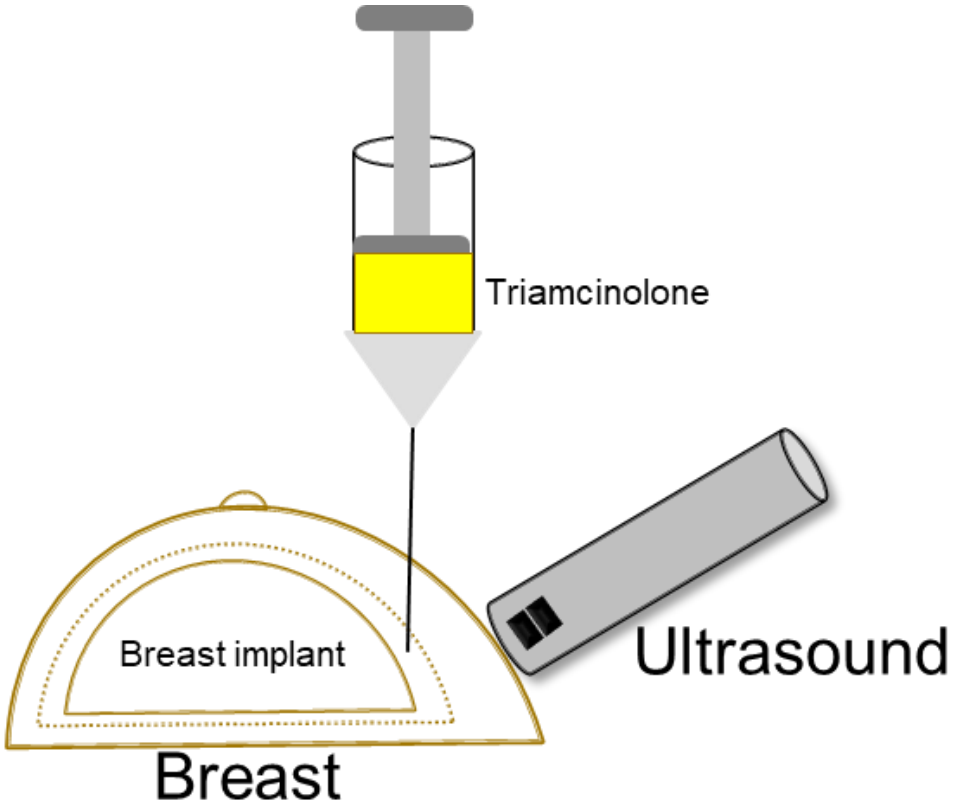

Figure 1.2. Schematic drawing of the surgical procedure. The needle tip is inserted into a capsule of the implant under ultrasound guidance. Dotted line = contracted capsule.

1.3 Research Aims

In this dissertation, my major goal was to develop the strand-based controllable drug delivery carrier that could maintain functionality of the original medical device and be applicable to medical devices of various sizes and shapes. To this end, using the electrospinning and electro-spraying methods, I fabricated drug delivery sheets with anti-inflammatory drugs. Thereafter, the drug delivery strands were prepared by cutting the sheets to a certain width based on the specific requirements of the medical device application. The strands had individual mechanical properties, such as rigidity and flexibility, and the controlled drug release was enabled by the use of different polymers or the polymer to drug ratios. Moreover, in order to ensure biocompatibility, a bio-polymer was used. Finally, due to the individual covering system on the medical device, the strands also acquired the anti-inflammatory effect. Due to these advantages of strands, the strand-based controllable drug delivery carrier can be applicable to many medical devices of various sizes and shapes.

In Chapter 2 of the present dissertation, I report the development of a surgical suture that could release the drug in a sustained manner to relieve the local, persistent inflammation around a surgical wound site. As mentioned above, the mechanical strength

is a crucial characteristic of a suture, as the major function of surgical sutures is to close the wound or connect organs and tissues. Considering that, due to the natural human body reaction, using a suture can easily induce inflammation around the wound site, inflammation-related pain is inevitable until natural healing is completed. This emphasizes the need of a controllable drug delivery system that would carry the anti-inflammation drug to the wound site and release it until recovery is completed. In the present study, I accurately delivered the non-steroidal anti-inflammatory drug (NSAID) to reduce inflammation and pain during an acute inflammatory period that normally requires a larger amount of the drug to reduce severe pain. To this end, using the electro-spraying method, I fabricated a strand of 1.5 mm in width with diclofenac; thereafter, this strand was physically braided around the surgical suture to maintain the mechanical strength. The fabricated controllable drug delivery strand can consistently release the drug until the natural healing process is over, to ensure that pain is successfully suppressed throughout the inflammatory period. Due to the simple physical attachment of the strand, its mechanical strength is preserved.

In Chapter 3, I report creating the elastic sheet of polyurethane and triamcinolone (glucocorticoid) using the electrospinning method to be further used for the drug delivery of

silicone implant. This elastic sheet was also cut the strands 3 mm in width strand, and 4 of these strands were crossed to make an elastic net. Since silicone implants require the elasticity that can mimic the human body, the fabricated elastic net also had to mimic the mechanical properties of the silicone implant. Furthermore, silicone implant has a wide range of volume depending on the body types and patients' demands. To meet these requirements and to cover the entire range of clinically used silicone implants, each of the fabricated elastic strands had to be enlarged by more than 100 percent in length. Additionally, the drug delivery elastic net could control the drug delivery system regardless of whether or not the net was stretched. As shown by the results, the fabricated elastic net could deliver triamcinolone for 4 weeks of the acute inflammatory phase. During this period, as revealed by the results, the production of inflammatory cytokines and fibrosis that typically occurs in the chronic inflammatory phase could both be successfully suppressed.

In summary, in the present study, I developed a controllable drug delivery strand to be attached to surgical sutures and silicone implants without any degradation in physical properties. In medical applications, surgical sutures are used to close and connect tissues, while silicone implants are frequently used during breast reconstruction, which causes a large wound when they are inserted. Under these circumstances, inflammation that causes pain, scars,

abnormal fibrosis, and capsular contractures is inevitable. In order to rule out inflammation and its side effects, I developed a drug delivery carrier based on strands to suppress inflammation around the implanted sites.

Testing the fabricated strand-based delivery carrier to be attached to surgical sutures and silicone implants shows that the carrier did not compromise the functionality of medical devices and did not require any further modification of medical devices.

Chapter 2

Surgical Suture Braided with a Diclofenac-loaded Strand for Local, Sustained Pain Mitigation

2.1 Introduction

To treat local, surgical pain in clinical settings, patients are often prescribed drugs, such as nonsteroidal anti-inflammatory drugs (NSAIDs), to be administered systemically via the oral route or injection (32, 33). As pain generally persists after surgery, long-term, repeated drug administrations are required until the surgical wounds have completed healing. Such long-term systemic drug exposure can cause adverse side effects, including Reye's syndrome, platelet dysfunction and renal impairment (34, 35). Moreover, for oral administration, drug bioavailability, especially at the local level in the wounded site of interest, could be low due to the first-pass metabolism of the liver (36, 37). Therefore, to be effective, frequent oral administrations or high drug doses are often needed, which may cause gastric hemorrhage, ulcer perforation or gastrointestinal tract obstruction (38, 39).

As such, local drug delivery is considered advantageous for treating pain at surgical wound sites. Therefore, in this study, I pursued to alleviate the pain via local drug delivery only in a way of promoting the pain relief efficacy, as well as minimizing the side effects possibly caused by conventional systemic drug exposure. In this sense, surgical sutures can be considered good candidate devices for incorporation with local drug-delivery functionality. Sutures could close wounds while concurrently relieving pain via local drug release. Many surgical sutures already available for clinical use are made of

various biocompatible polymers, such as polycaprolactone, polydioxanone, poly(lactic acid), poly(glycolic acid) and poly(lactic-co-glycolic acid) (PLGA) (40-42). Sutures eluting the anti-infective drug, triclosan, have already been commercialized (20). For drug elution, sutures have mostly been dip-coated in a drug solution (11-14, 26). However, this strategy may degenerate the inherent mechanical properties of the suture, which are required for proper wound closure (14).

The sustained release of a pain-reliever is advantageous for treating pain persisting during wound healing. However, this type of release is not easily achievable via conventional dip-coating processes (43). Therefore, I propose a biodegradable surgical suture that is physically braided with a drug-delivery carrier to allow local, sustained drug release while maintaining its own mechanical properties. To accomplish this, I separately fabricated a polymer strand containing a pain-relief drug and physically braided it with a commercially available surgical suture (VICRYL™, Ethicon, USA). According to this approach, I could modulate drug-release scenarios by varying the drug-delivery strand without affecting the suture itself. In this study, I employed diclofenac (DF) as an NSAID pain-reliever (44). DF is a COX-2-specific targeted inhibitor that reduces the secretion of prostaglandin, which is a known factor involved in the generation of pain (45, 46). For pain-relief indications, DF is already

approved for clinical use via both oral administration and injection (47, 48).

In this work, to achieve sustained drug release, I first prepared a sheet by electrospraying a solution containing a blend of the biodegradable polymer, PLGA and DF. The drug-loaded sheet was then cut into strands to be braided with a surgical suture (VICRYL™ W9114, Ethicon, USA). I characterized the drug-delivery strand via X-ray diffraction and Fourier transform infrared (FTIR) spectroscopic analyses. To examine the mechanical properties of the suture braided with the drug-delivery strand (i.e., the drug-delivery suture), a tensile strength test was performed. The drug-delivery suture was also applied in an induced-pain rat model to examine *in vivo* pain-relief efficacy.

2.2 Materials and Methods

2.2.1 Materials

PLGA (50:50; end-capped; average MW = 58 kDa; inherent viscosity = 0.41 dl/g) was obtained from Lakeshore Biomaterials (Birmingham, USA). Diclofenac sodium and phosphoric acid were purchased from Sigma-Aldrich (MO, USA). The biodegradable surgical sutures (3-0 VICRYL™ W9114) were purchased from Ethicon (NJ, USA). Dimethylformamide (DMF), dichloromethane (DCM), potassiumphosphate and sodium hydroxide (NaOH) were acquired from Daejung (Siheung, Korea). Acetonitrile (ACN) was purchased from JT Baker (NJ, USA). Zoletil 50 was purchased from Virbac (TX, USA), and xylazine was purchased from Bayer (Lerverkusen, Germany). Paraformaldehyde (4%) was supplied from Korea CFC (Ansan, Korea). For the hematoxylin and eosin (H&E) staining, xylene, ethanol and hydrochloric acid (35-37%) were purchased from Duksan Pure Chemicals (Ansan, Korea). Ammonia solution (28-30%) was obtained from Junsie Chemical (Tokyo, Japan). Modified Mayer's Hematoxylin and Eosin Y solutions were supplied by Richard-Allan Scientific (MI, USA). Paraffin was supplied from Merck (NJ, USA).

2.2.2 Fabrication of Drug-delivery Strands and Sutures

In this work, I first prepared a PLGA sheet loaded with DF. For this, both PLGA (4% w/v) and DF (5% w/w) were dissolved in a solvent mixed with DMF and DCM (1:100, v/v), and the solution was then electrosprayed for 3 h under the following conditions (Nano NC, Siheung, Korea): voltage, 25 kV; infusion rate, 10 ml/h; distance between tip and collector, 10 cm; and needle, 24 G. I also prepared a sheet of PLGA only as a control by electrospraying a PLGA solution in DCM (4% w/v) under the same conditions stated above. The resulting sheet was cut into strands, 1.5 mm in width, which were then braided with a VICRYL™ surgical suture, as shown in Figure 2.1. Thus, I prepared two distinct strands: the strand cut from a PLGA sheet loaded with DF (i.e., the PLGA_DF strand) and the strand cut from a sheet of PLGA only (i.e., the PLGA strand). The assembled sutures were treated at 47 ºC for 1 h to improve strand attachment and were then sterilized using an ethylene oxide gas (49). Thus, I employed three distinct sutures in this work: the intact VICRYL™ suture (i.e., the original suture); the suture assembled with a PLGA_DF strand (i.e., the PLGA_DF suture); and the suture with a PLGA strand (i.e., the PLGA suture).

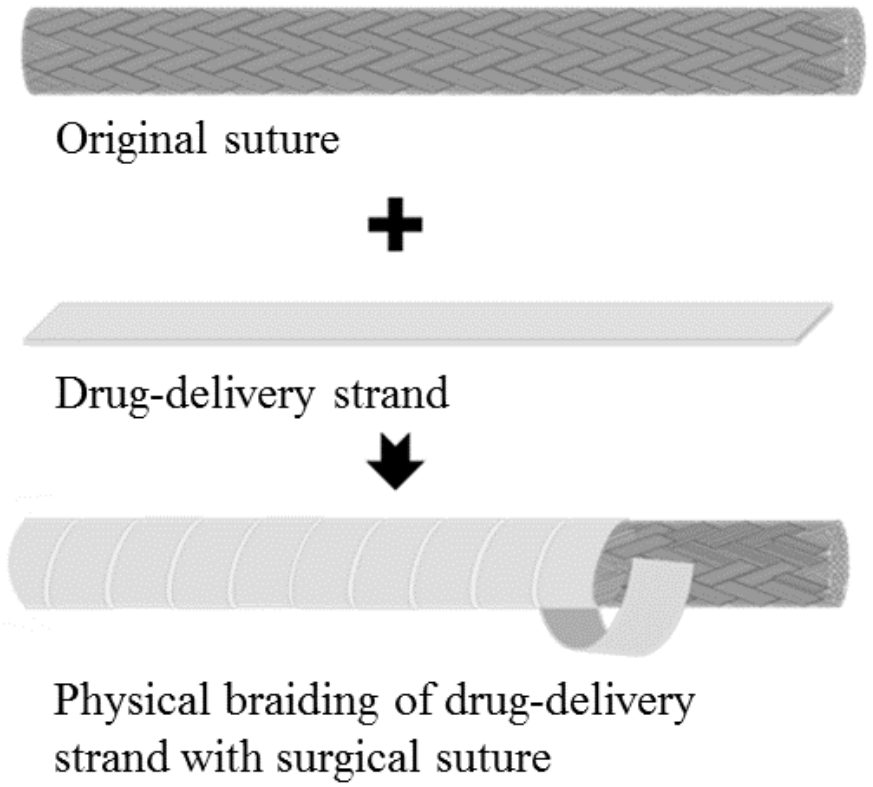

Figure 2.1. Schematic showing the process of preparing the drug-delivery suture.

2.2.3 Characterization Methods

To measure the thickness of a strand, 5 different locations from a single strand were randomly selected and measured using a micrometer (Mitutoyo America, IL, USA). To examine the presence of DF and PLGA, the strand was examined by FTIR (JASCO, Japan) in a range of 400–4000 cm^{-1} with a resolution of 4 cm^{-1} using the KBr disk method. The strands were also assessed with an X-ray diffractometer (D/MAXRINT 220-Ultima, Rigaku, Japan), where Ni-filtered CuK_{α} radiation at a wavelength of 1.5418 Å was used to scan the samples at a constant rate of 2 °/min and a tube voltage of 40 kV with a current of 30 mA. To measure the residual solvent, 8 mg of the PLGA_DF strand was fully dissolved in chloroform, and 2 μl of the resulting solution was assessed with gas chromatography–mass spectrometry (GC–MS; Agilent technologies 7890B/5977A GC/MSD, USA) under selected ion monitoring mode using an Agilent DB-624 column (30 m × 0.25 mm × 1.4 μm). During measurement, the flow rate was set at 1 ml/min, and the temperature was increased from 50 °C to 100 °C at a rate of 5 °C/min and from 100 °C to 240 °C at a rate of 20 °C/min.

I imaged all the sutures with scanning electron microscopy (SEM; 7501F, JEOL, Japan). To investigate the mechanical properties of the sutures, the straight- and knot-pull tests were performed

using a universal testing machine (UTM; Instron 5543, MA, USA) with a 1-kN load cell (50); the sutures were pulled at a cross-head speed of 200 mm/min. In addition, I dip-coated original suture for 2 hours in various organic solvent such as DCM, DMF, ethyl acetate, ethanol and tetrahydrofuran to compare the ultimate mechanical strength of sutures (14). To measure the amount of loaded DF, 4 cm of the PLGA_DF suture was fully dissolved in 10 ml of DMF, an aliquot of which was measured at 276 nm with a spectrophotometer (UV-1800, Shimadzu, Japan) (51).

2.2.4 *In vitro* Drug-release Study

To examine the *in vitro* drug release profiles, the PLGA_DF suture was cut into 1-cm pieces, and 4 randomly selected pieces were placed into 1 ml of pH 7.4 phosphate-buffered saline (PBS), which was shaken at 125 rpm at 37 ° C. At the scheduled times of 1, 2, 3, 5, 7 and 10 days, 1-ml aliquots were collected and replaced by an equal volume of fresh PBS. The aliquot was measured via high-performance liquid chromatography (HPLC; 1260 Infinity Quaternary LC system, Agilent, CA, USA) with a C_{18} analytical column (150 mm × 4.6 mm; 5 μm) (52). The UV detection was set at 270 nm, and the mobile phase consisted of ACN and 20 mM PBS at pH 2.5 (40:60, v/v).

2.2.5 *In vivo* Pain-relief Evaluation

To evaluate pain relief *in vivo*, I prepared an induced-pain animal model based on the protocol I used in a previous study (53). For this evaluation, 9-week-old Sprague-Dawley rats were used, and the animals were maintained under a 12-h light/dark cycle with free access to food and water. All *in vivo* procedures were approved by the Institutional Animal Care and Use Committee at Seoul National University Bundang Hospital (BA1309-137-082-01). In brief, to prepare an induced-pain animal model, the animals were anesthetized via an intraperitoneal injection of zoletil and xylazine (1:1 v/v) cocktail at 1 ml/kg. Then, the skin on the right leg was incised to expose the quadriceps femoris muscle, which was then incised to prepare a wound 1 cm in length and 2 cm in depth. The animals with induced pain were divided into three distinct groups, i.e., that in which the muscle wound was sutured with 4 cm of the original suture, the PLGA suture or the PLGA_DF suture. While suturing, detachment of the strand was not observed. For all groups, the skin was closed with a nylon 4-0 suture (Ethicon, USA). I prepared a sham animal group, where no incision was made in the muscle, and only the skin on the right leg was incised and sutured with a nylon 4-0 suture. For all animals, the incision site was disinfected with iodine solution. Therefore, a total of five different animal groups were employed in

this work: the naïve (i.e., the untreated), sham, original suture, PLGA suture and PLGA_DF suture groups. Five animals were assigned to each animal group; hence, a total of 25 animals were used in this study. To evaluate pain relief, I examined the motility of the animals by measuring the rearing count and movement velocity (54). For 5 min on each scheduled day, I counted the instances of rearing, which were defined as when infrared beams set at 12 cm above the ground (Photo-beam & Video motion analysis, In Electronics Design, Korea) were disrupted. The movement velocity of the animals was measured 1 day after surgery. For this, I recorded the movement of the animal with a camera (HVR3300CA, High Vision, Korea) while it walked through a transparent cage (150 cm × 13 cm × 16 cm).

2.2.6 Histological Evaluation

For the histological evaluation, tissue including the suture was biopsied 14 days after surgery. The tissue was fixed in 4% paraformaldehyde, and after 1 day, it was treated with xylene and ethanol. Subsequently, the tissue was paraffinized and sliced into 4-μm-thick sections using a microtome. These sections were stained with H&E, imaged, and then analyzed by a professional pathologist (×4; Carl Zeiss, Germany). To evaluate the degree of inflammation, the images were each scored semi-quantitatively (0: none; 1: mild;

2: moderate; and 3: severe) (55). For the quantitative analysis, I also measured the thickness of the inflammatory region around the suture; in each image, I found and measured the shortest length between the boundary of the suture and the end point of inflammatory region around the suture (56). At least five animals were examined per animal group.

2.2.7 Statistical Analysis

To compare the rearing counts and velocities among the four different animal groups (i.e., the sham, original suture, PLGA suture and PLGA_DF suture groups), the Kruskal–Wallis test followed by the Bonferroni correction was performed ($p < 0.05$) (57). The Kruskal–Wallis test was also performed to compare the inflammation grades and thicknesses of the inflammatory region among the animal groups ($p < 0.05$).

2.3 Results and Discussion

2.3.1 Characterization of Strands and Sutures

In this study, I first prepared PLGA and PLGA_DF strands via electrospraying, and their thicknesses were measured to be 46.0 ± 0.8 μm and 47.6 ± 1.9 μm, respectively. I assessed the FTIR spectra to examine the presence of PLGA and DF in the strands, as shown in Figure 2.2. For the intact PLGA, the absorption band strongly appeared at 1762 cm^{-1} due to C=O stretching vibrations (58), and the band found at 3545 cm^{-1} represented hydroxyl (O–H) stretching (59); these bands were also observed for both the PLGA and PLGA_DF strands. For the intact DF, the characteristic bands appeared at 1504 cm^{-1} and 745 cm^{-1} due to the C=C stretching in the aromatic rings and the C–Cl stretching, respectively (60, 61). The characteristic bands of both intact PLGA and DF were observed to be overlapped in the spectra of the PLGA_DF strand. According to the X–ray diffraction patterns shown in Figure 2.3, the characteristic peaks were observed with intact, crystalline DF (62), while the intact PLGA and PLGA strands did not exhibit these peaks due to the amorphous nature of PLGA (63). For the PLGA_DF strand, the characteristic peaks observed for the intact DF were absent, suggesting a noncrystalline, molecular–level distribution of DF in the

strand (62). Regarding residual solvent, DCM was not detected and 10.54 ppm of DMF was measured in the PLGA_DF strand, which was much lower than the amount of DMF permitted in pharmaceuticals (880 ppm) (64). However, future study is needed to develop a proper drying procedure to further remove residual DMF.

In this work, I braided a PLGA or PLGA_DF strand around a VICRYL™ surgical suture and observed the resulting cross-sections via SEM. As shown in Figure 2.4 and 2.5, the original VICRYL™ suture used herein was composed of multiple filaments. In addition, for the PLGA and PLGA_DF sutures, the braided strand around the suture was clearly observed. To examine the mechanical properties of the sutures, I performed the straight- and knot-pull tests using a UTM. As shown in Table 2.1, the ultimate tensile strength of both the PLGA and PLGA_DF sutures did not decrease compared with the original suture. However, the ultimate tensile strength of other dip coated suture groups decreased compared with the original suture. The amount of DF loaded in the PLGA_DF suture was measured to be 23.7 ± 1.2 μg/cm. To a large extent, the mechanical strength of the PLGA_DF used herein originated from the core suture of the body, i.e., the original VICRYL™ suture. When implanted, the PLGA_DF strand present at the suture surface would degrade faster than the VICRYL™ suture due to its lower density: the strand was made by electrospraying a polymer and drug solution while the VICRYL™

suture was made by melt-spinning. In this sense, the breaking strength retention (BSR) or bioabsorption profile of the PLGA_DF herein would depend mostly on that of the original VICRYL™ suture. However, evaluating the BSR profile will be important, for the commercialization of this material (65).

According to the *in vitro* drug-release profile shown in Figure 2.6, the PLGA_DF suture released approximately 90% of the loaded DF (i.e., 21.4 ± 0.2 μg/cm) in a sustained manner for the first 3 days; subsequently, the rest of DF was slowly released until 10 days. As determined by visual examination, no sutures became disassembled or broken during this period. Additionally, when the drug concentration was measured using HPLC, the retention time was not observed to be shifted, suggesting that the DF was stable for 10 days. In my previous work, I also separately fabricated a polymeric strand loaded with ibuprofen via electrospinning to prepare a drug-delivery surgical suture (53). However, the strand possessed a nanofibrous structure, and due to its high porosity, prolonged drug release was not easily obtained. To resolve this, I adopted a more complicated, multiple-step electrospinning procedure, which could fabricate additional layers as drug-diffusion barriers around the strand. In the current work, the strands were prepared via electrospraying, where small droplets of a polymer and drug solution were sprayed and deposited to form a denser structure in the strand

instead of forming nanofibers (66). Therefore, although the water solubility of DF herein (39 mg/ml) (67) was much higher than that of ibuprofen (0.06 mg/ml) (68), the electrosprayed strand prepared in this work allowed for more-sustained drug release even using a single-step electrospraying procedure.

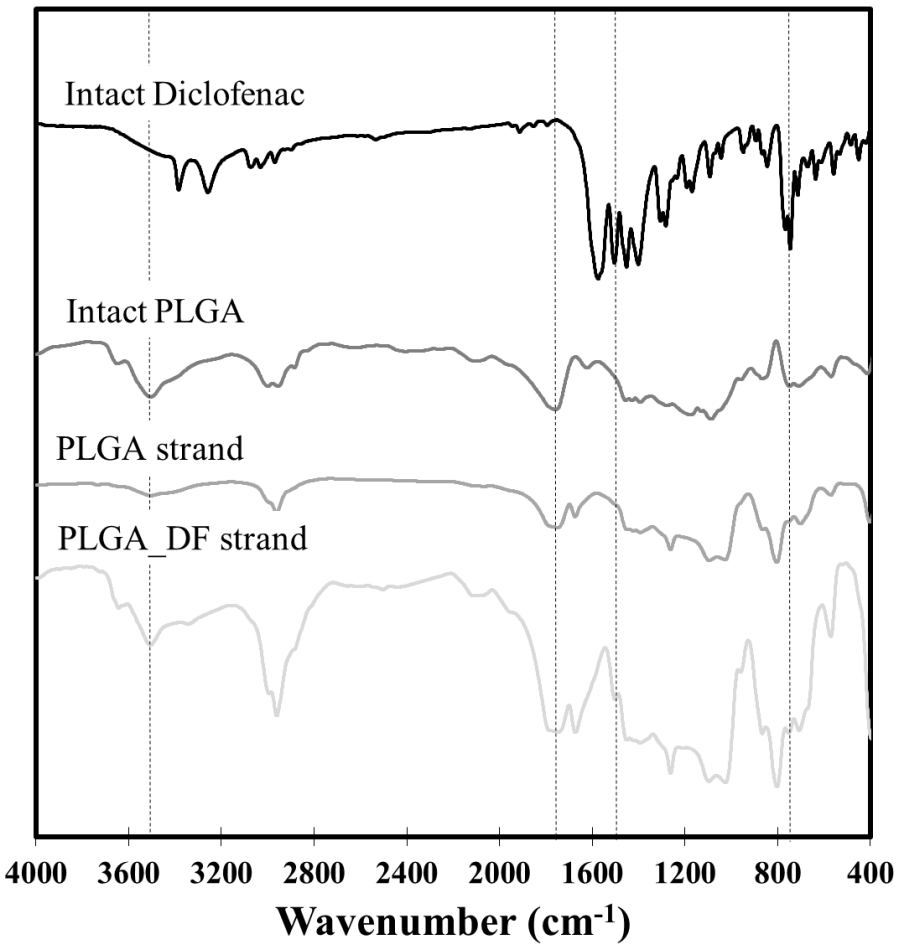

Figure 2.2. Fourier transform infrared spectra of intact DF, intact PLGA, PLGA strand and PLGA_DF strand.

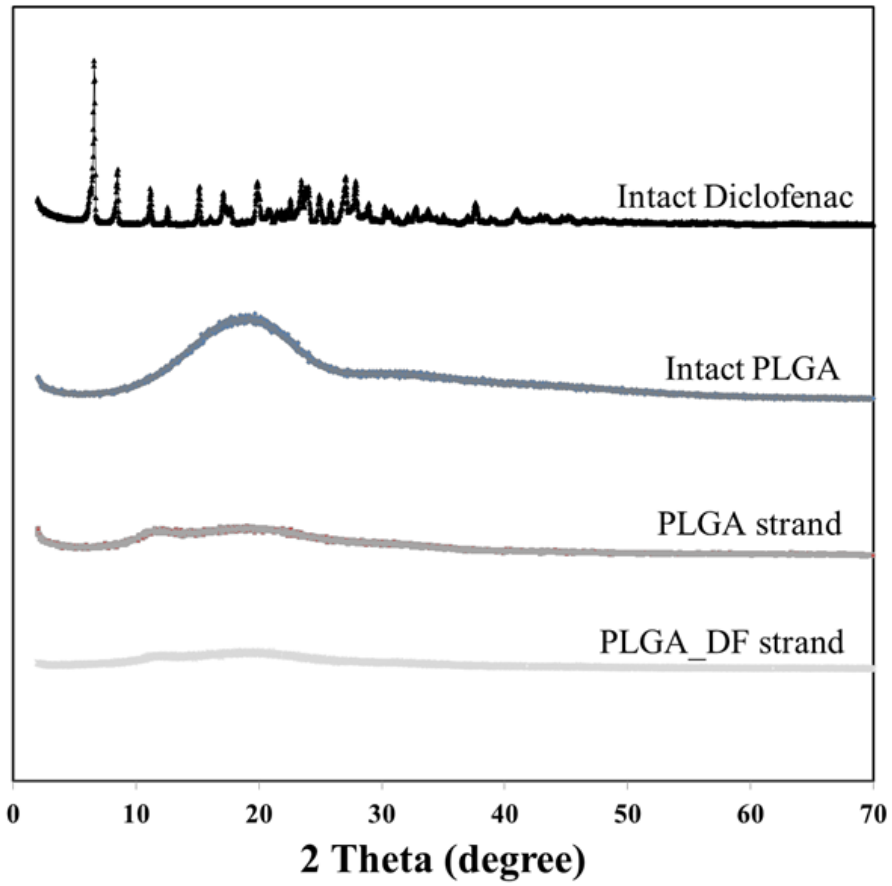

Figure 2.3. X-ray diffraction patterns of intact DF, intact PLGA, PLGA strand and PLGA_DF strand.

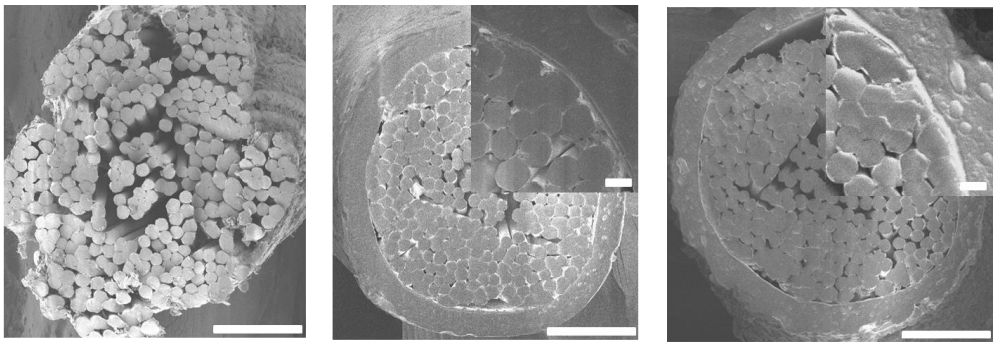

Figure 2.4. Cross-sectional SEM images of (a) original suture, (b) PLGA suture and (c) PLGA_DF suture. The inserts in (b) and (c) show more detailed images of the sutures obtained at larger magnification. The scale bars in the main images and insets are 100 μm and 10 μm, respectively.

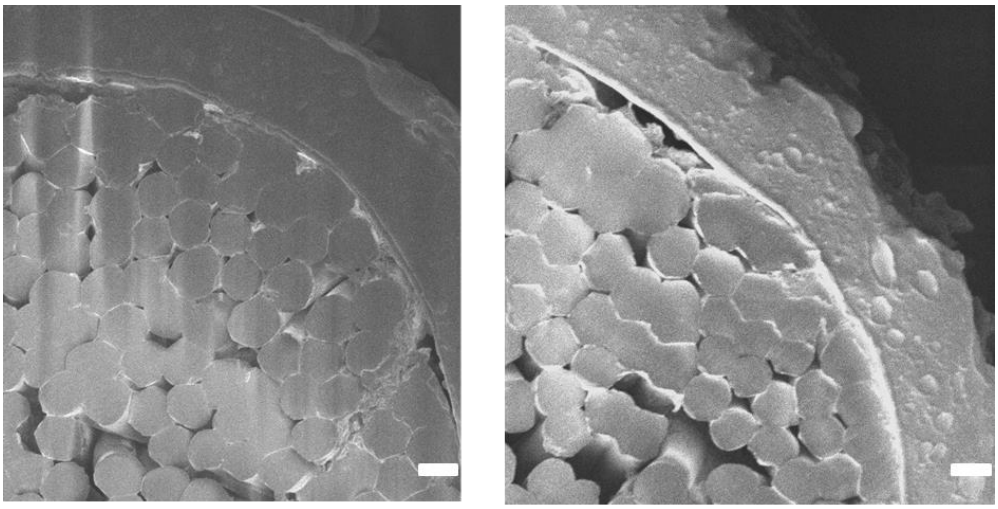

Figure 2.5. Cross-sectional SEM images of (a) PLGA suture and (b) PLGA_DF suture, which are the larger images of the insets in Figure 2.4 (b) and (c), respectively. The scale bars are 10 μm.

Table 2.1. Mechanical properties of the sutures

Test	Suture type	Tensile strength at break (N)
Straight-pull test	Original suture	42.61 ± 1.33
	PLGA suture	42.19 ± 3.31
	PLGA_DF suture	43.95 ± 1.48
Knot-pull test	Original suture	22.95 ± 1.12
	PLGA suture	22.40 ± 1.61
	PLGA_DF suture	23.28 ± 1.89
Straight-pull test	Suture dip-coated in DCM	38.35 ± 1.02
	Suture dip-coated in DMF	38.00 ± 1.14
	Suture dip-coated in THF	38.14 ± 1.18
	Suture dip-coated in Ethyl Acetate	38.80 ± 2.74
	Suture dip-coated in Ethanol	39.89 ± 0.56

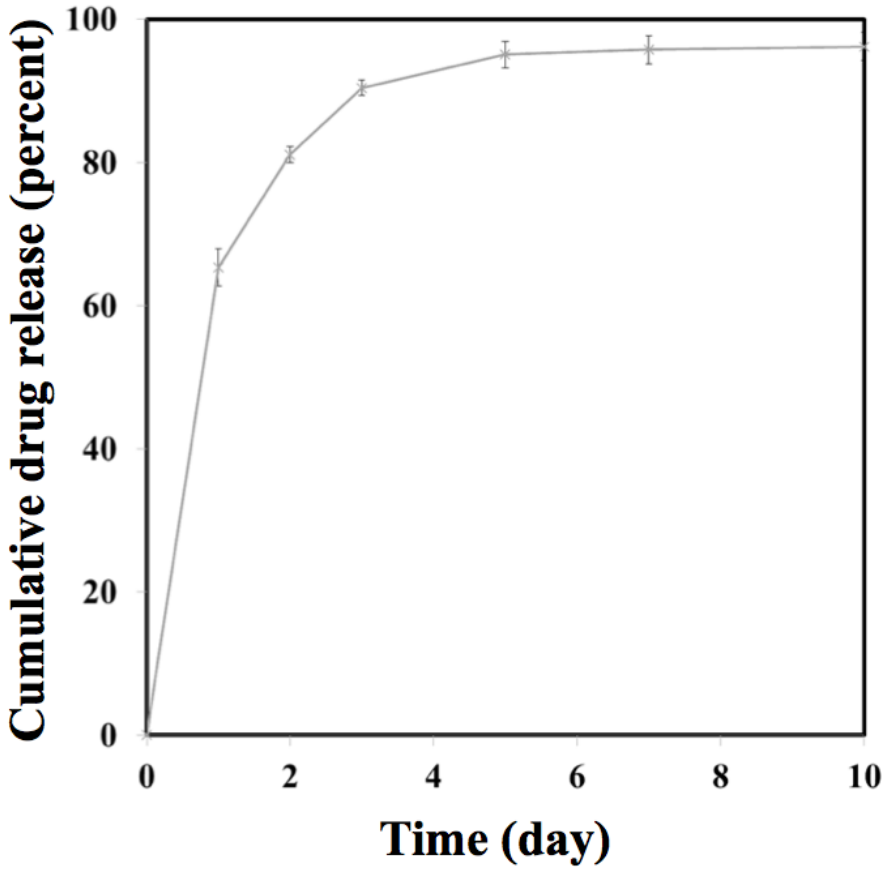

Figure 2.6. *In vitro* drug release profiles of the PLGA_DF suture.

2.3.2 *In vivo* Efficacy Evaluation

To evaluate pain relief, I first assessed the rearing activity of the animals with induced pain treated with the different sutures described herein and compared this activity with that of the sham group (53). A higher rearing activity suggested less pain, and vice versa. As shown in Figure 2.7, the rearing counts of both the original and PLGA suture groups, where the muscle incision was treated with the suture without DF, were significantly lower than that of the sham group up to 7 days, indicating the presence of untreated, prominent pain. After 9 days, the rearing counts became more similar, as the wounds had healed to a large extent. However, for the PLGA_DF suture group, the rearing activity was continuously similar to that of the sham group throughout the testing period, including the first 7 days after surgery. This result suggests that the PLGA_DF suture presented herein could mitigate the pain throughout the wound-healing period via sustained drug release (Figure 2.6)

I also examined the velocity of the animals with induced pain treated with the different sutures on 1 day after surgery, when the presence of relatively high pain was expected. Thus, a higher velocity suggested less pain, and vice versa. I compared the velocity profile of the suture groups with that of the sham group, where only the skin was incised and thus, there was no pain induced in the muscle. As

shown in Figure 2.8, the original and PLGA suture groups exhibited velocities significantly lower than that of the sham group, suggesting the presence of untreated pain. However, for the PLGA_DF suture group, the velocity was more similar to that of the sham group and was higher than those of the original and PLGA suture groups. This result suggested that the DF released on the first day could properly mitigate the relatively high pain experienced in the short-term after surgery.

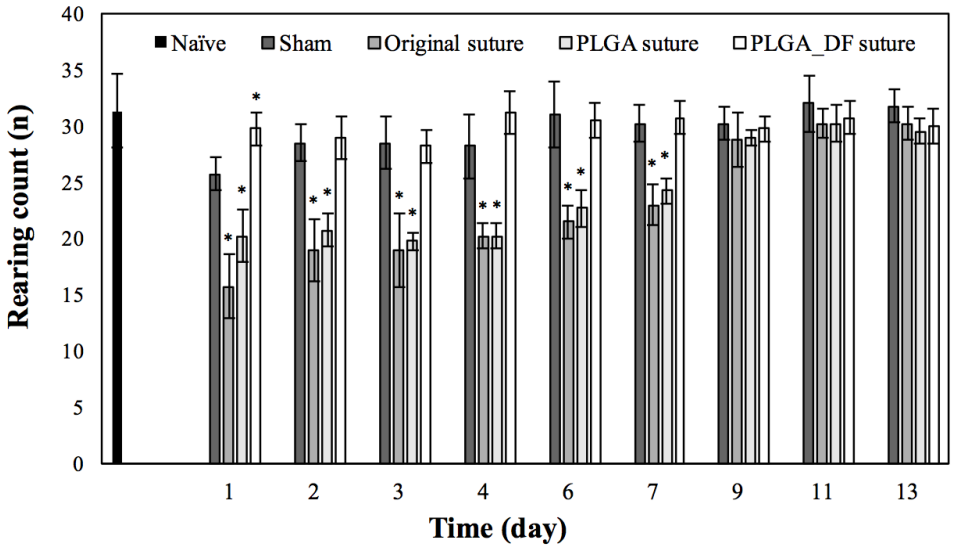

Figure 2.7. Rearing activity obtained in the animal groups; * $p<0.05$, significantly different from the sham group.

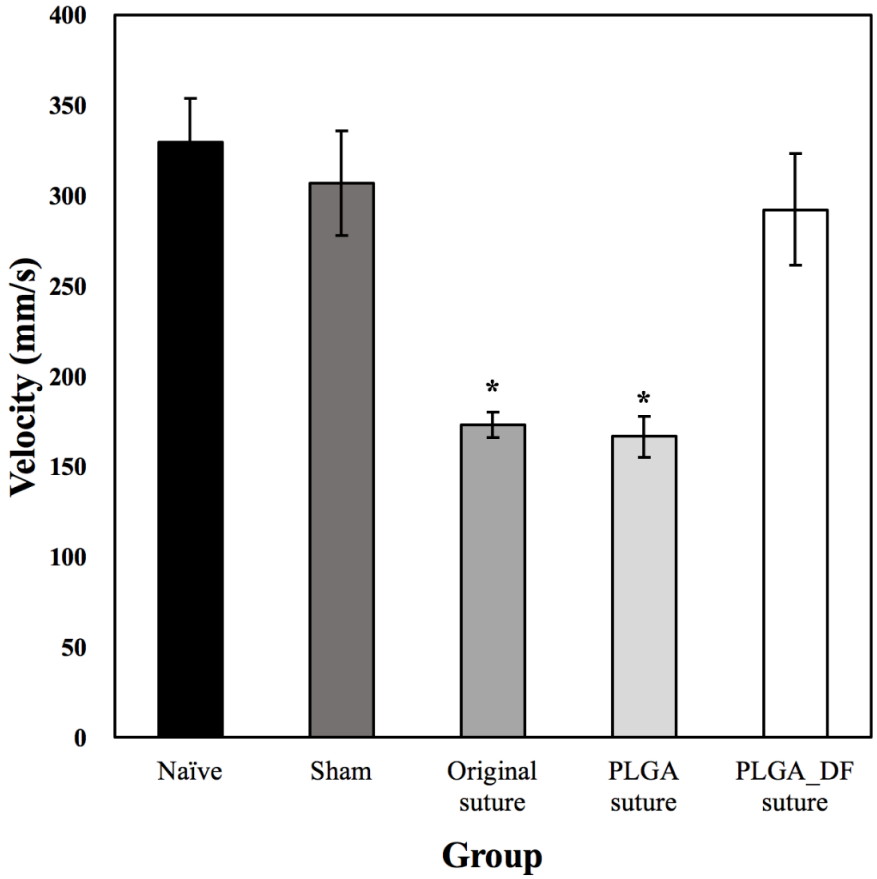

Figure 2.8. Velocity profiles obtained in the animal groups at 1 day after surgery; * $p<0.05$, significantly different from the sham group.

2.3.3 Histological Evaluation

To examine the biocompatibility and anti-inflammatory effect of DF, I performed a histological analysis of the tissues around the original, PLGA and PLGA_DF sutures, which were biopsied at the end point of the experiment, i.e., 14 days after surgery. As shown in Figure 2.9, for all suture groups, inflammation was indeed present probably due to the acidic by-products of PLGA degradation. However, the PLGA_DF suture group exhibited significantly lower inflammation scores and inflammatory tissue thicknesses compared with the original suture group. These results suggested that a sustained, local release of DF indeed exerted an anti-inflammatory effect on the surrounding tissue, suppressing inflammatory cell recruitment and activation (69). This decreased inflammation also suggests that the biocompatibility of the PLGA_DF suture is comparable to that of the original VICRYL™ suture already approved for clinical use.

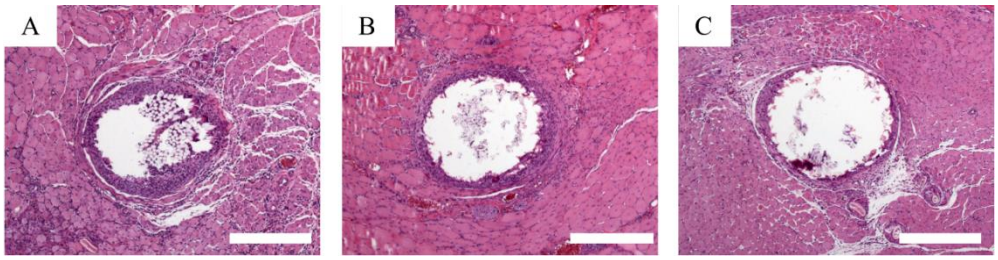
A
B
C

(a)

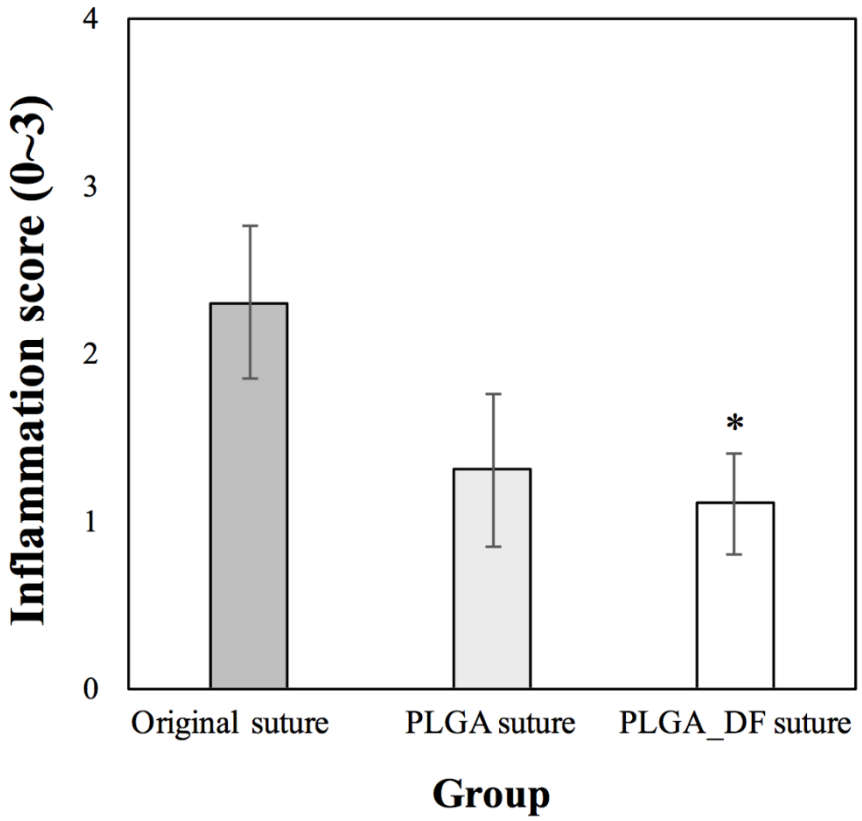
Inflammation score (0~3)
4
3
2
1
0
*
Original suture
PLGA suture
PLGA_DF suture
Group

(b)

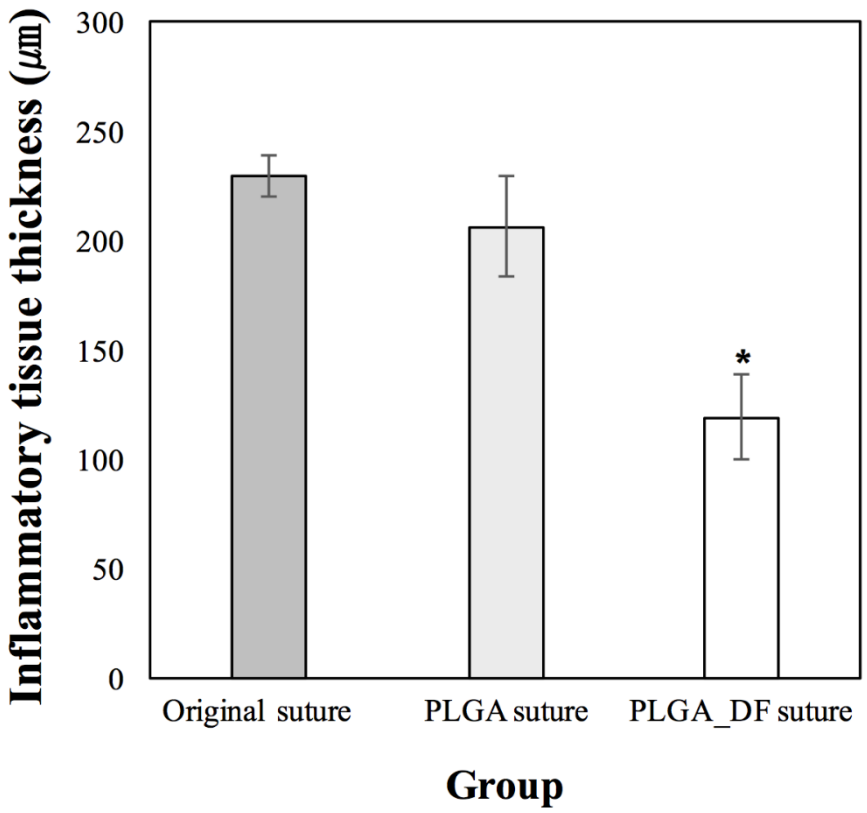

(c)

Figure 2.9. Histological analysis of the tissues around the sutures, based on H&E staining. The tissues were biopsied 14 days after surgery. (a) Representative histological images (A: original suture, B: PLGA suture and C: PLGA_DF suture). The scale bars are 100 μm. (b) Inflammation grade scores and (c) inflammatory tissue thicknesses; *<0.05, significantly different from the sham group.

2.4 Conclusion

In this study, I developed a surgical suture that could release DF in a sustained manner to relieve the local, persistent pain present around a surgical wound site. I aimed to attain this drug-delivery functionality while retaining the inherent mechanical strength of the surgical suture. Therefore, I separately prepared a drug-loaded strand via electrospraying a solution containing both DF and PLGA and physically braided it with a surgical suture already in clinical use. As a result, the drug-delivery suture presented herein could release DF in a sustained manner for up to 10 days, and its mechanical properties were not degraded compared with the original surgical suture in clinical use. My *in vivo* experimental results revealed that this drug-delivery suture could decrease pain throughout the tested period and that it possesses good biocompatibility. Therefore, I conclude that a surgical suture braided with a polymeric strand loaded with a pain-reliever is a promising device for the treatment of local pain at surgical wound sites.

Chapter 3

Elastic Net of Polyurethane Strand for Sustained Release of Triamcinolone Around Silicone Implant of Various Sizes

3.1 Introduction

Silicone implants are medical devices utilized for augmentation and reconstruction in clinical settings (70–72). However, capsular contracture around inserted implants has been one of the most severe complications (73–75). It has been reported that up to 30% of patients experience capsular contracture, and more than 10% of those patients need replacement surgery, which can increase the chance of surgery–related risks as well as the financial burden for the patients (73, 76–78).

Capsular contracture results mostly from pathological fibrosis, which originates from an upregulated and prolonged inflammatory response around an implant (4, 79, 80). Thus, the implant is eventually surrounded by excessive fibrotic tissue and thereby isolated from the body. At first, the wound from the implantation procedure causes acute inflammation at the surgical site, where polymorphonuclear leukocytes (PMNs) secrete numerous proinflammatory cytokines (4, 81). Due to the presence of a large wound along with a nondegradable implant, acute inflammation can become chronic, in which fibroblasts are recruited and activated by cytokines, such as transforming growth factor–β (TGF–β), and excessive collagen bundles are synthesized around the implant (82, 83). TGF–β also causes fibroblasts to differentiate into

myofibroblasts, which contract collagen bundles, causing capsular contracture around the implant (84).

Therefore, the local delivery of an anti-inflammatory drug around a silicone implant would be beneficial for modulating the upregulated inflammation and thus preventing capsular contracture (85, 86). Considering the occurrence of prolonged inflammation due to silicone implants, sustained drug release would be more advantageous, and polymeric coatings have often been employed over the entire surface of silicone implants to serve the purpose of a drug-diffusion mediator (7, 86, 87). However, from manufacturing perspective, silicone implants are produced in a variety of sizes (88, 89); thus, for each implant size, a specific coating process may need to be developed to optimize the coating stability and the drug dose.

Therefore, to be applicable to silicone implants of various sizes, I propose an elastic net made of a biocompatible polymer as a local, sustained drug delivery carrier. In this work, a drug-delivery net (DDN) was made of elastic strands of polyurethane loaded with an anti-inflammatory drug, triamcinolone, which is known to suppress fibrosis around silicone implants (29, 30, 90). Thus, I hypothesized that due to the elastic property of the DDN, DDNs of a single size carrying the same triamcinolone dose could tightly wrap silicone implants of various sizes and still release triamcinolone in a sustained manner locally from the surface of the implant to prevent fibrosis.

To test the DDN herein, I prepared implant samples using polydimethylsiloxane (PDMS) with volumes of 1 ml and 7 ml, representing the smallest and largest volumes of the silicone breast implants often employed in clinical settings, respectively (91–93). Thus, the DDN was prepared to just fit the 1 ml sample but was also applied to the 7 ml sample. To evaluate the efficacy of the DDN, the different implant samples, which were wrapped with DDNs of the same size and triamcinolone dose, were each inserted subcutaneously in living rats. Then, the tissue was biopsied at scheduled times for 12 weeks to analyze inflammation and fibrosis.

3.2 Materials and Method

3.2.1 Materials

A kit for a silicone elastomer with a PDMS base and curing agent was obtained from Dow Corning (SYLGARD 184, USA). Polyurethane and acetonitrile (ACN) were purchased from Sigma-Aldrich (USA) and Fisher Scientific (USA), respectively. Triamcinolone (TA) and 1,1,1,3,3,3-hexafluoro-2-propanol (HFP) were purchased from Tokyo Chemical Industry (Japan). I obtained dimethylformamide (DMF) and ammonium acetate from Dae-Jung (Korea). Isoflurane was purchased from Hana Pharm (Korea). Paraffin and paraformaldehyde (4%) solutions were obtained from Merck (USA) and KCFC (Korea), respectively. Xylene and ethanol were supplied from Duksan Pure Chemical (Korea). Mayer-modified hematoxylin and eosin Y solutions were purchased from Thermo Fisher Scientific (USA). I obtained biebrich scarlet-acid fuchsin, phosphomolybdic acid, phosphotungstic acid, aniline blue and hydrochloric acid from Merck (USA). VECTASHIELD was supplied by Vector Laboratories (USA). An antigen-retrieval solution (10X) and antibody diluent were obtained from Dako (USA). Anti-TGF-β (sc-146) and anti-vimentin antibodies were supplied by Santa Cruz Biotechnology (USA) and Abcam (UK), respectively. I purchased

Alexa Fluor® 488 (A11001) from Life Technologies (USA).

3.2.2 Preparation of Silicone Samples and DDN

While I prepared small silicone implant samples suitable for implantation in living rats, the volume range and shape mimicked those of implants in clinical use (91, 92). Thus, I prepared two different hemispherical molds, 2 and 4 cm in diameter, into which the PDMS base was poured and cured at 100 ºC for 1 h to produce samples of approximately 1 ml and 7 ml, respectively. The 1 ml and 7 ml samples (i.e., the SI and LI, respectively) represented the smallest and largest volumes of silicone breast implants in clinical use (88). To prepare the DDN herein, a solution dissolved with polyurethane (8% w/v) and triamcinolone (5% w/w) was prepared in HFP, which was electrospun (Nano NC, Korea) to produce a polyurethane sheet loaded with triamcinolone. The electrospinning conditions were as follows: voltage, 20 kV; infusion rate, 1 ml/h; distance between tip and collector, 10 cm; needle gauge, 20 G; and duration, 5 h. As a control, a sheet of polyurethane was also fabricated to produce the elastic net without triamcinolone (i.e., the EN), for which the solution of polyurethane in HFP (8% w/v) was electrospun under the same conditions described above. I cut the resulting sheet into strands 3 mm in width and 6 cm in length, four of which were rolled and attached

by heat to prepare the net, as depicted in Figure 3.1e. I prepared six different implant samples: a 1 ml implant without the net (i.e., the SI); a 7 ml implant without the net (i.e., the LI); a 1 ml implant wrapped with the EN (i.e., the EN_SI); a 7 ml implant wrapped with the EN (i.e., the EN_LI); a 1 ml implant wrapped with the DDN (i.e., the DDN_SI); and a 7 ml implant wrapped with the DDN (i.e., the DDN_LI).

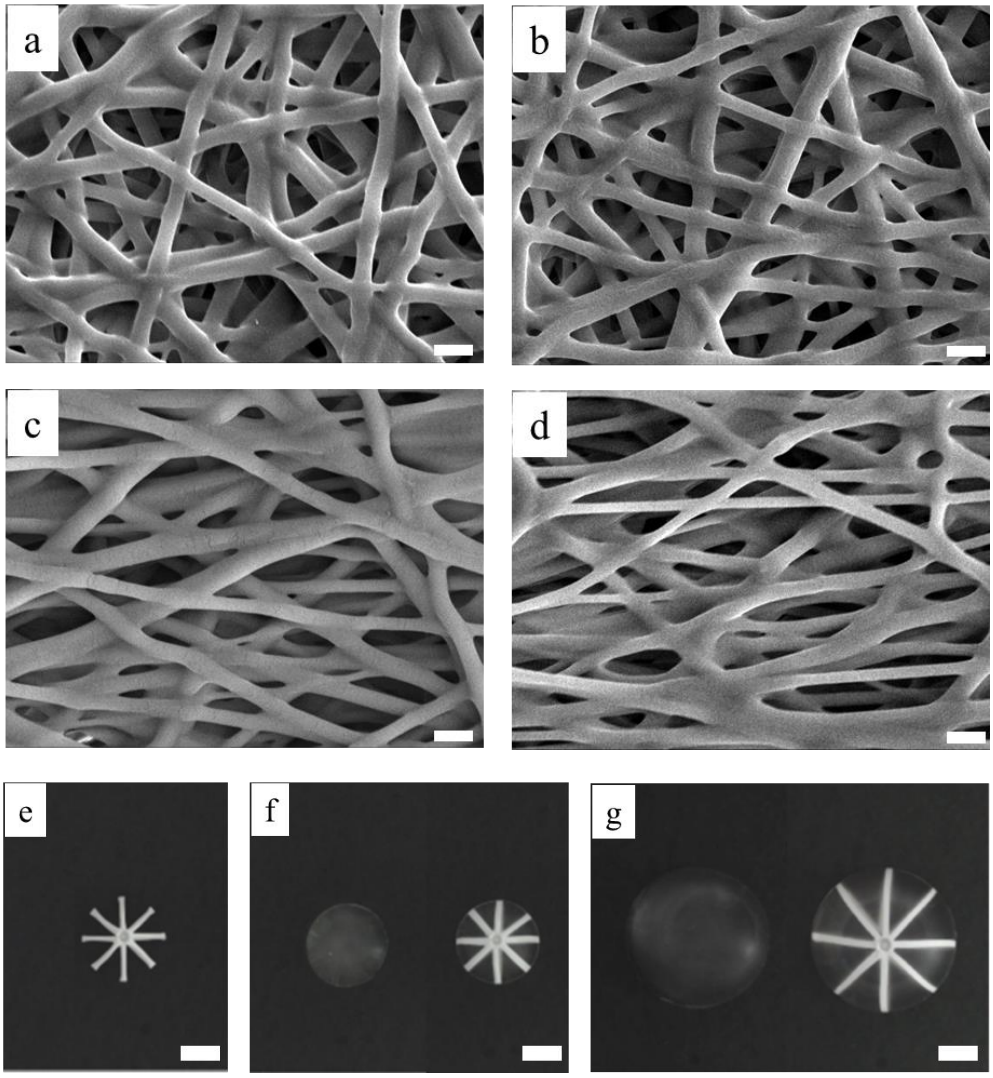

Figure 3.1. Scanning electron micrographs of the surfaces of the strands for (a) EN_SI, (b) DDN_SI, (c) EN_LI and (d) DDN_LI. Scale bars are 1 μm. and optical images of (e) DDN, (f) SI and DDN_SI, and (g) LI and DDN_LI. Scale bars are 1 cm.

3.2.3 Characterizations

To assess the morphology, I observed each of the strands of the EN and DDN by scanning electron microscopy (SEM; 7800F Prime, JEOL, Japan). Strands elongated up to 72% strain, which would be the maximum strain needed to wrap the LI sample in this work, were also examined. To evaluate the mechanical properties, the strands were subjected to a straight-pull test with a universal testing machine (UTM; Instron-5543, Instron, USA). The strands were also evaluated by X-ray diffractometer (XRD; D/MAX RINT 220-Ultima, Rigaku, Japan) under Ni-filtered CuK_{α} radiation at a wavelength of 1.5418 Å; the samples were scanned at a constant rate of 2 °/min at a tube voltage and current of 40 kV and 30 mA, respectively. I also optically observed and imaged the nets, intact implant samples, and net-wrapped implant samples using a camera (HD Pro Webcam C920r, Logitech, Switzerland). To measure the loaded amount of triamcinolone, 1 cm of the strand material composing the DDN was dissolved in 5 ml of DMF, and the concentration of triamcinolone was measured by high-performance liquid chromatography-mass spectrometry (HPLC-MS; 1260 series, Agilent Technologies, USA) using a C_{18} analytical column (Poroshell, 2.7-μm pore size, 4.6 x 100 mm, Agilent Technologies) under the following conditions: flow rate, 5 ml/min; and injection volume, 10 μl. For this examination, I prepared

the mobile phase by mixing 2 mM ammonium acetate at pH 3.2 and ACN (55:45, v/v).

3.2.4 *In vitro* Drug Release Study

To assess the drug release behavior, *in vitro* drug release experiments were conducted for the implant samples wrapped with the DDN, i.e., the DDN_SI and DDN_LI. Each sample was fully submerged in pH 7.4 PBS (10 ml) at 37 ° C under shaking at 125 rpm in an incubator (SI-600R; JeioTech, Korea). At predetermined time points up to 28 days, the whole volume of release medium (10 ml) was fully extracted and replaced with fresh PBS. The triamcinolone concentration in the obtained medium was measured by HPLC-MS as described above. The experiment was repeated three times for DDN_SI and DDN_LI.

3.2.5 *In vivo* Experiments

For the *in vivo* evaluation, I used male Sprague-Dawley rats (8 weeks old, 250-300 g), which were maintained under a 12/12 h light/dark cycle in a specific-pathogen-free (SPF) laboratory with free access to food and water. The experimental protocol was approved by the Institutional Animal Care and Use Committee of Seoul

National University Bundang Hospital (approval number: BA1102-077/006-01), and all procedures were in accordance with the NIH Guide for the Care and Use of Laboratory Animals. I assigned the animals to six different groups according to implant type, i.e., the SI, LI, EN_SI, EN_LI, DDN_SI and DDN_LI groups, with 8 animals in each group.

For implantation, the animal was first anesthetized by isoflurane inhalation. Then, the fur on the dorsal region was removed, and the skin was then disinfected with 70% alcohol and betadine. After making a skin incision, the sample was inserted into the subcutaneous pocket, and the incision was closed with nylon 4/0 surgical sutures (Ethicon, USA), followed by disinfection. At 2 and 8 weeks after implantation, four animals per group were sacrificed via carbon dioxide inhalation to biopsy the tissue around the sample.

3.2.6 Histological and Immunofluorescence Analysis

For this evaluation, the biopsied tissue was fixed in 4% paraformaldehyde, embedded in paraffin, and sectioned at 4 μm for staining. For evaluation of the capsule, skin and muscle thickness, and inflammation degree, the sections were stained with hematoxylin and eosin (H&E). Each section was treated with hematoxylin solution and then washed with water. Next, the section was treated with 0.3% HCl

and 70% ethanol and was then dipped into a 0.1% ammonium hydroxide solution. Finally, the section was treated with eosin Y solution and dehydrated sequentially with ethanol and xylene. The section was then observed and imaged at x50 magnification (Imager A1; Carl Zeiss, Germany). To assess the capsule thickness, I measured the thinnest region of the capsule tissue (94, 95). The thickness of the skin and muscle was measured in three distinct, randomly selected regions for each corresponding tissue. To examine the inflammation degree, each section was observed at x200 magnification and scored semiquantitatively, as follows: 0; none, 1; mild, 2; moderate, and 3; severe.

To evaluate the collagen density, each section was stained with Masson's trichrome (MT) by sequential treatment with biebrich scarlet-acid fuchsin, phosphotungstic-phosphomolybdic acid and aniline blue. To determine the collagen density, images of the sections were obtained at x400 magnification, and the area of blue color (ImageJ software, NIH, USA) was calibrated as a percentage based on the area of the whole image. To assess the number of fibroblasts and the degree of TGF-β expression, immunofluorescence (IF) staining was conducted according to the manufacture's instructions using primary anti-vimentin and anti-TGF antibodies, respectively, at a dilution of 1:250 (55). To stain the cell nuclei, the sections were also treated with VECTASHIELD mounting medium containing DAPI.

Thus, for the IF-stained sections, the green and blue double-positive cells were counted in images obtained at x400 magnification. To assess the degree of TGF-β expression, the images were scored semiquantitatively, as follows: 0; none, 1; mild, 2; low, 3; medium, 4; high, and 5: severe.

For the EN and LI samples, which were not wrapped, 8 images were analyzed at each biopsy time. For the wrapped samples, two distinct areas of tissue that was in contact with the surface of the net (+) or bare silicone (-) were assessed; thus, a total of 16 images (i.e., 8 images for each tissue area) were assessed at each biopsy time. Therefore, there were five different tissue groups for each implant size: SI, EN_SI(+), EN_SI(-), DDN_SI(+) and DDN_SI(-) for the 1 ml implant; and LI, EN_LI(+), EN_LI(-), DDN_LI(+) and DDN_LI(-) for the 7 ml implant. The images were analyzed by a professional pathologist in a blinded manner.

3.2.7 Statistical Analysis

For each implant size, the nonparametric Kruskal-Wallis test was used to compare the evaluated values among the five tissue groups for dependent variables, which included the biopsy time and observed tissue area for each implant type. The evaluated values were the thicknesses of the capsule, skin and muscle, the collagen

density, the scores of inflammation and TGF−β expression, and the number of fibroblasts, respectively. Then, comparisons were made between two of the five tissue groups using the Mann–Whitney U test and Bonferroni correction, where $P < 0.01$ was considered statistically significant.

3.3 Results

3.3.1 Strand Characterization

To prepare the EN and DDN, I first fabricated strands of polyurethane and strands of polyurethane and triamcinolone, respectively, via electrospinning. Therefore, all strands herein were composed of nanofibers regardless of the presence of triamcinolone (Figures 3.1a–d). When the strands were elongated enough to be able to wrap the LI (72% strain), the nanofibers in the EN and DDN were observed to be slightly stretched; however, the strands did not exhibit major defects or cracks (Figures 3.1c, d). Due to the randomly oriented direction of the nanofibers, the strain applied to each nanofiber appeared to be lower than that applied to the whole strand in a single longitudinal direction (96). The 72% strain needed to wrap the LI was much lower than the maximum strain at break of the EN and DDN strands, which was measured to be 265.97 ± 23.94% and 281.28 ± 36.36, respectively. With those strands, I prepared the EN and DDN, as shown in Figure 3.1e, in a size just sufficient to wrap the SI (Figure 3.1f). Due to the elastic property of the polyurethane, the same size DDN could also wrap the larger LI sample, as shown in Figure 3.1g.

The XRD results in Figure 3.2 demonstrate the presence of

triamcinolone, as indicated by characteristic peaks originating from its crystallinity (97); however, there were no apparent peaks in the pattern of the strand used for the EN, without triamcinolone, due to the amorphous nature of the polyurethane (98). The pattern of the strand used for the DDN also did not exhibit the characteristic peaks even with the presence of triamcinolone, which suggested that the triamcinolone was distributed at a molecular level without crystal formation when loaded in the strand. For the DDN strand, the amount of loaded triamcinolone was measured to be 1.38 ± 0.07 μg/cm.

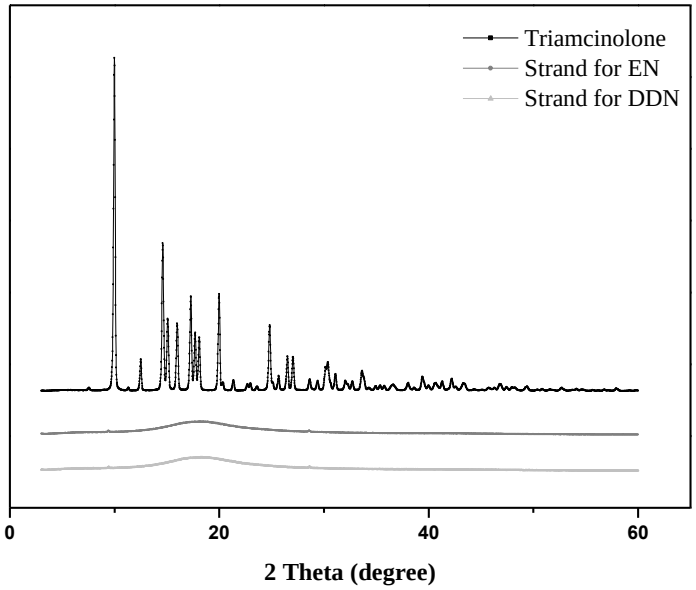

Figure 3.2. X-ray diffraction patterns of intact triamcinolone, and the strands for EN and DDN.

3.3.2 *In vitro* Release Profiles of Triamcinolone

I carried out in vitro drug release studies using implant samples of both sizes, each wrapped with the same DDN, i.e., DDN_SI and DDN_LI, both of which exhibited a similar pattern of sustained drug release for up to 28 days (Figure 3.3). The strain applied to the DDN to wrap the larger LI herein did not appear to influence the drug release property of the nanofibers in the DDN. The initial burst release on the first day could be ascribed to the drug present at the strand surface. Subsequently, the drug was released slowly at a rate of approximately 1.1%/day.

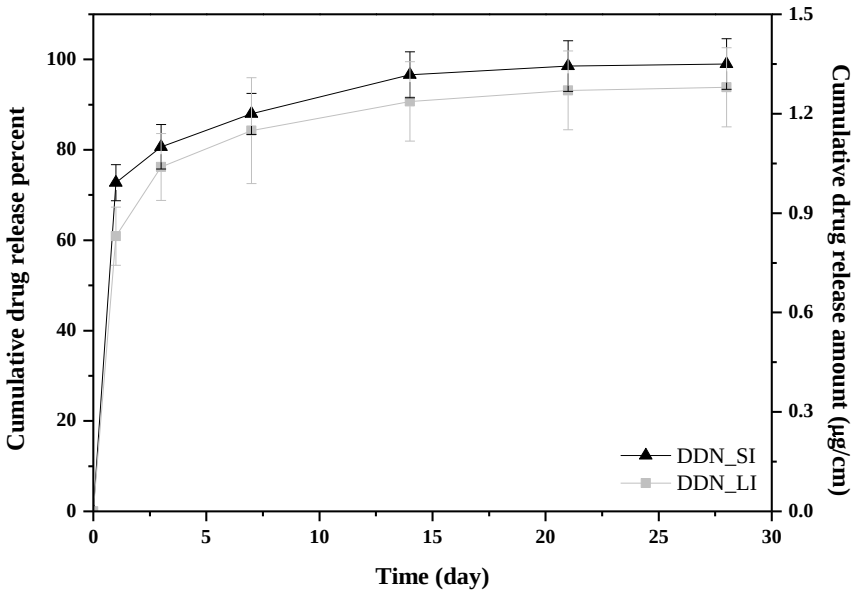

Figure 3.3. *In vitro* cumulative drug release profiles of the DDN_SI and DDN_LI plotted in percent and the amount.

3.3.3 *In vivo* Evaluation

To investigate the antifibrotic efficacy of triamcinolone, I assessed the capsule thickness around the implant samples prepared in this work, as shown in Figures 3.4a, b. At 2 weeks, a difference in the capsule thickness was not evident among the samples, as the capsule was be composed mostly of inflammatory cells. Thus, fibrosis was not yet fully developed at this early stage of inflammation (99). At 8 weeks, however, a decrease in capsule thickness was evident with the presence of triamcinolone, i.e., in both the DDN_SI and DDN_LI groups, compared with the SI and LI groups, respectively ($P < 0.01$). The density of collagen, a major constituent of fibrotic tissues, was also decreased in the DDN_SI and DDN_LI groups compared with the SI and LI groups, respectively (Figures 3.4c, d). For the samples wrapped with the EN, without the drug, both the capsule thickness and collagen density were similar to those of the unwrapped SI and LI samples, respectively ($P > 0.05$). I also examined the degree of TGF-β expression and the number of fibroblasts as a major cytokine and cell type involved in massive collagen synthesis during fibrosis (82). Figures 3.7 and 3.9 show that there was significantly lower TGF-β expression and fewer fibroblasts around all samples wrapped with the DDN ($P < 0.01$). In the EN_SI and EN_LI groups, these parameters were similar to those measured in the SI and LI group, respectively

($P > 0.05$).

It should be noted that for the samples wrapped with the DDN, the decrease in capsule thickness and collagen density was prominent, along with the decrease in TGF-β expression and fibroblast number; these values did not significantly differ according to sample size or tissue location ($P > 0.05$), i.e., tissue in contact with either the DDN or bare silicone surface. This result suggests that the same DDN could release the drug with similar efficacy over the entire surface of both implant sizes employed in this work. As shown in Figure 3.11, the overall inflammation was indeed lowered by the DDN regardless of the implant size and tissue location, which again suggests prolonged action of the anti-inflammatory drug, triamcinolone, over the entire surface of the implant sample.

Albeit effective for modulating inflammation, triamcinolone may cause muscle and skin thinning as side effects of overexposure (100-102). To assess the safety of the triamcinolone dose employed in this work, I examined the thickness of both the muscle and skin. As shown in Figure 3.13, no samples wrapped with the DDN exhibited a significant change in muscle or skin thickness compared with the intact SI and LI samples during the whole testing period of 8 weeks ($P > 0.05$).

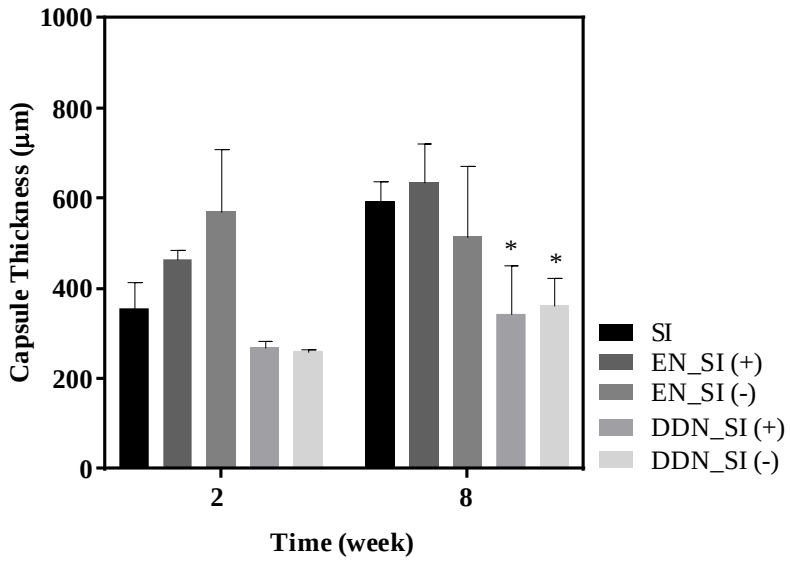
1000
800
600
400
200
0
Capsule Thickness (μm)
2
8
Time (week)
*
*
SI
EN_SI (+)
EN_SI (-)
DDN_SI (+)
DDN_SI (-)

(a1)

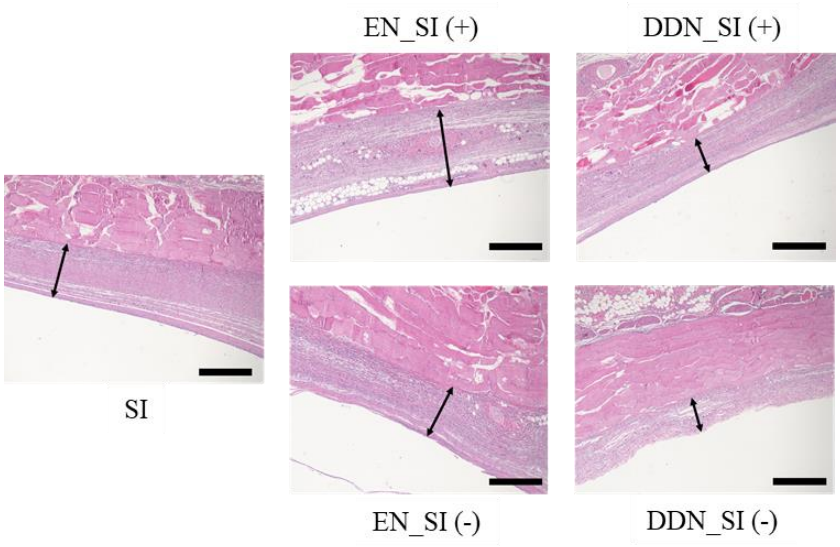
EN_SI (+)
DDN_SI (+)
SI
EN_SI (-)
DDN_SI (-)

(a2)

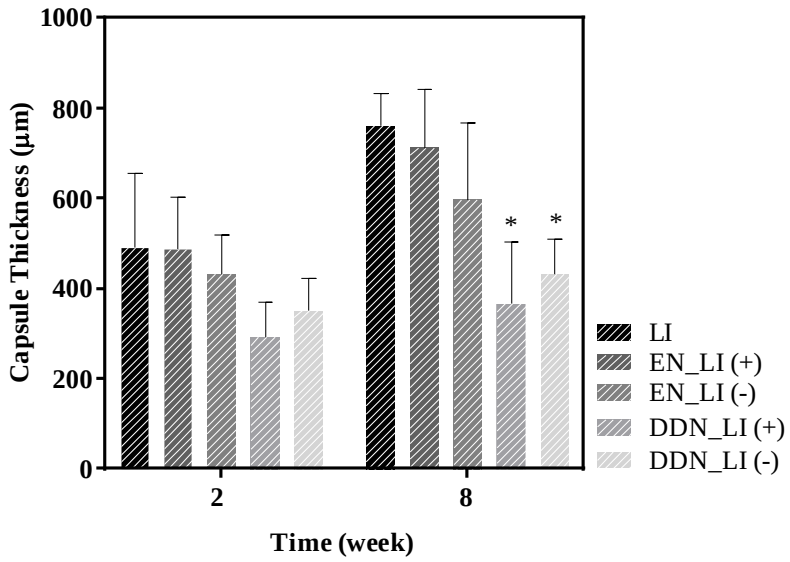
1000
800
600
400
200
0
Capsule Thickness (μm)
2
8
Time (week)
*
*
LI
EN_LI (+)
EN_LI (-)
DDN_LI (+)
DDN_LI (-)

(b1)

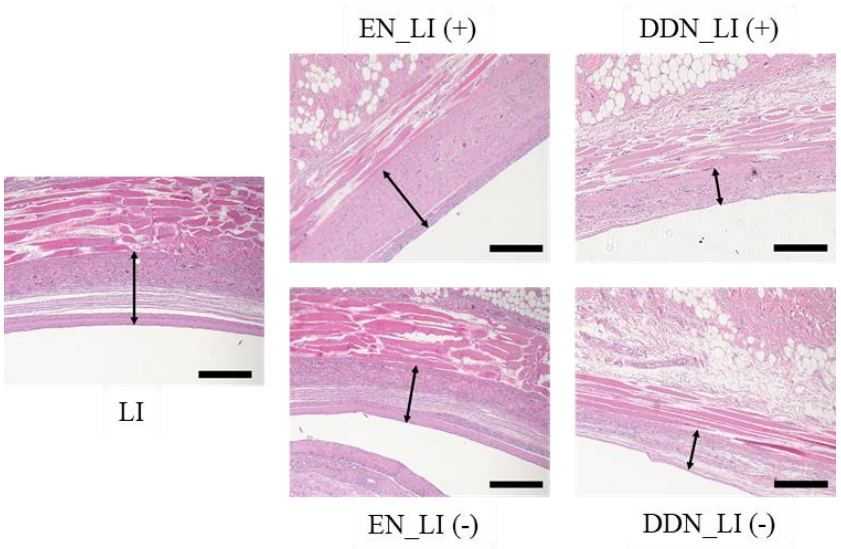
EN_LI (+)
DDN_LI (+)
LI
EN_LI (-)
DDN_LI (-)

(b2)

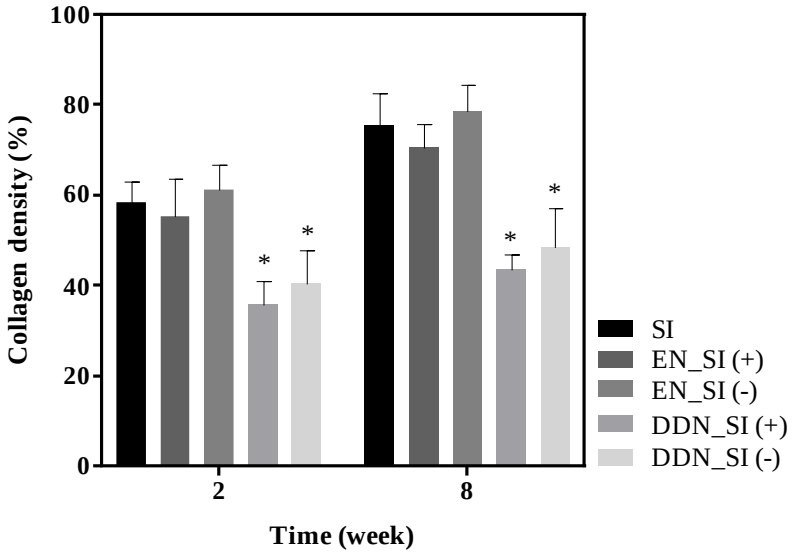
100
80
60
40
20
0
Collagen density (%)
2
8
Time (week)
*
*
*
*
SI
EN_SI (+)
EN_SI (-)
DDN_SI (+)
DDN_SI (-)

(c1)

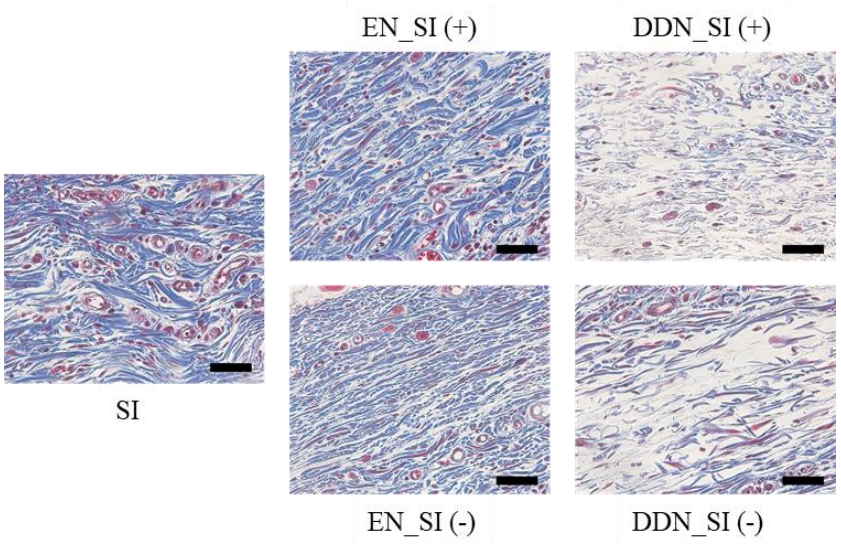
EN_SI (+)
DDN_SI (+)
SI
EN_SI (-)
DDN_SI (-)

(c2)

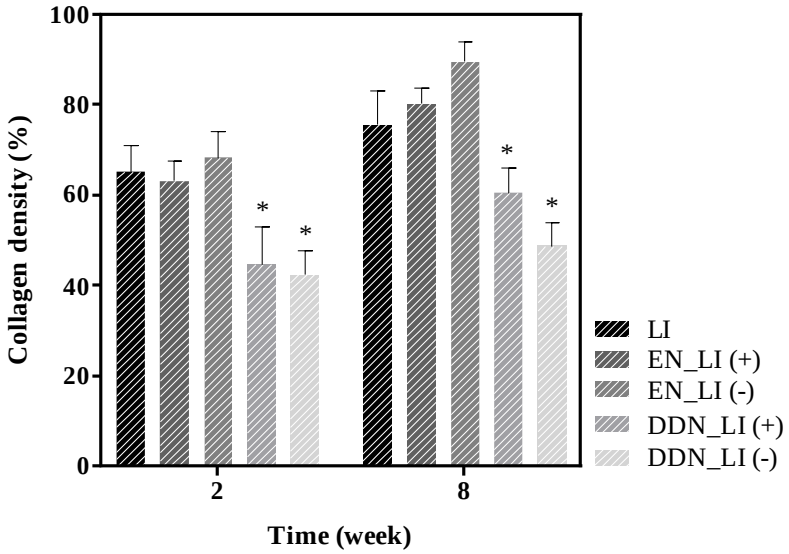
100
80
60
40
20
0
Collagen density (%)
2
8
Time (week)
*
*
*
*
LI
EN_LI (+)
EN_LI (-)
DDN_LI (+)
DDN_LI (-)

(d1)

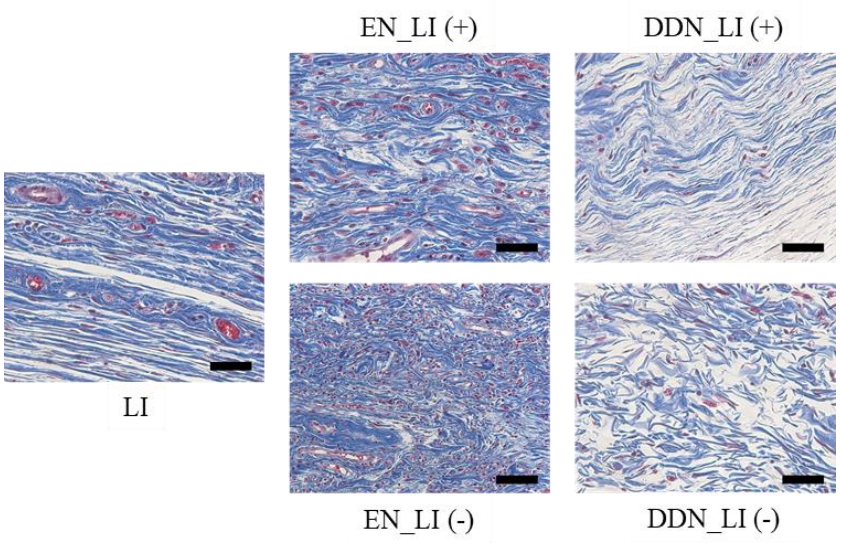
EN_LI (+)
DDN_LI (+)
LI
EN_LI (-)
DDN_LI (-)

(d2)

Figure 3.4. Evaluation of fibrotic capsules around the silicone implant samples. Profiles of capsule thickness in the tissues around the silicone implant samples of (a1) small and (b1) large sizes. Asterisk (*) represents a statistically significant difference compared with the intact SI and LI, respectively ($P < 0.01$). Representative H&E-stained images of the tissues around the silicone implant samples of (a2) small and (b2) large sizes obtained at 8 weeks after implantation. Black arrows indicate the capsule thickness. Scale bars are 500 μm. Profiles of collagen density in the tissues around the silicone implant samples of (c1) small and (d1) large sizes. Asterisk (*) represents a statistically significant difference compared with the intact SI and LI, respectively ($P < 0.01$). Representative MT-stained images of the tissues around the silicone implant samples of (c2) small and (d2) large sizes obtained at 8 weeks after implantation. Scale bars are 100 μm.

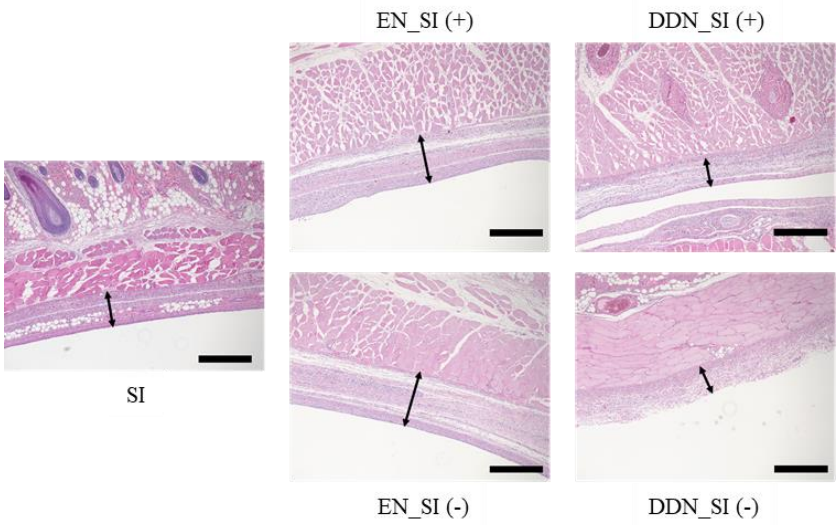

(a)

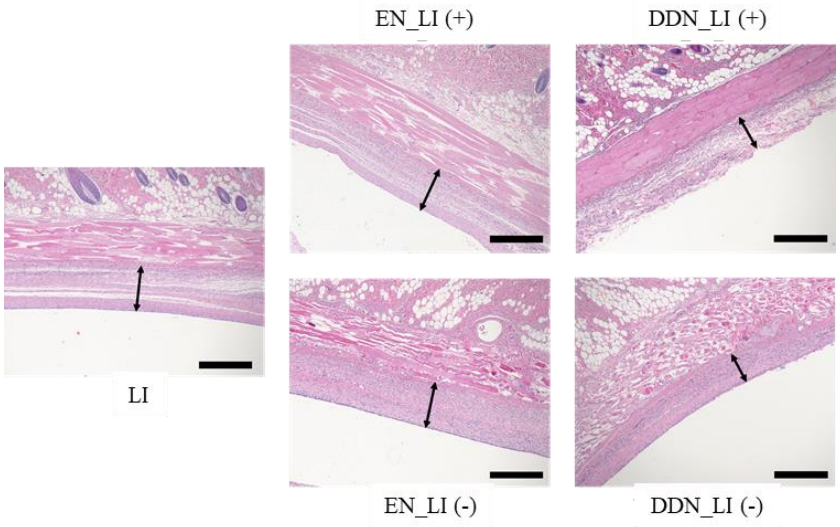

(b)

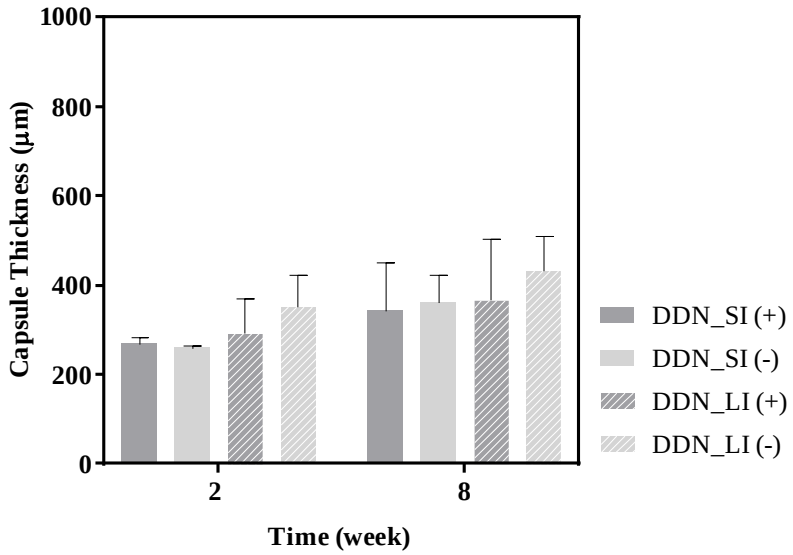

(c)

Figure 3.5. The capsule thickness around the silicone implants. Representative histological images of (a) SI and (b) LI groups obtained at 2 weeks after implantation. (c) show the comparison of DDN_SI and DDN_LI. The black arrows signify capsule thickness and the scale bars are 500 μm.

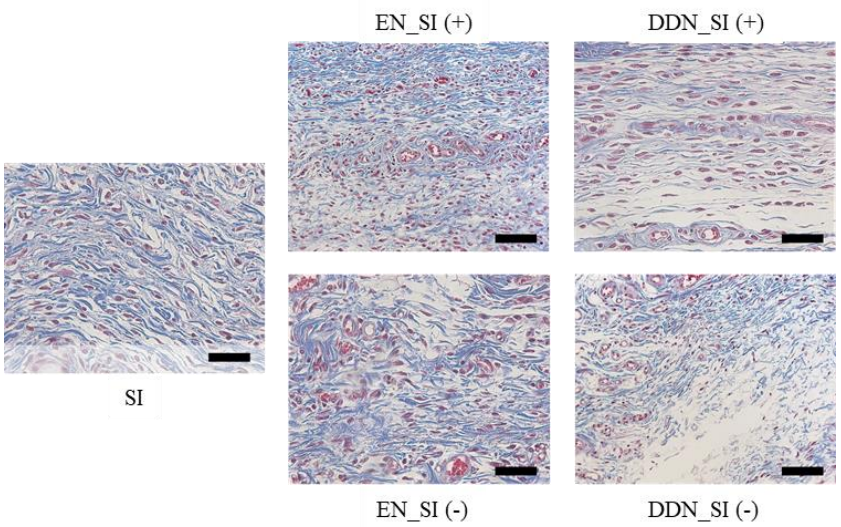

(a)

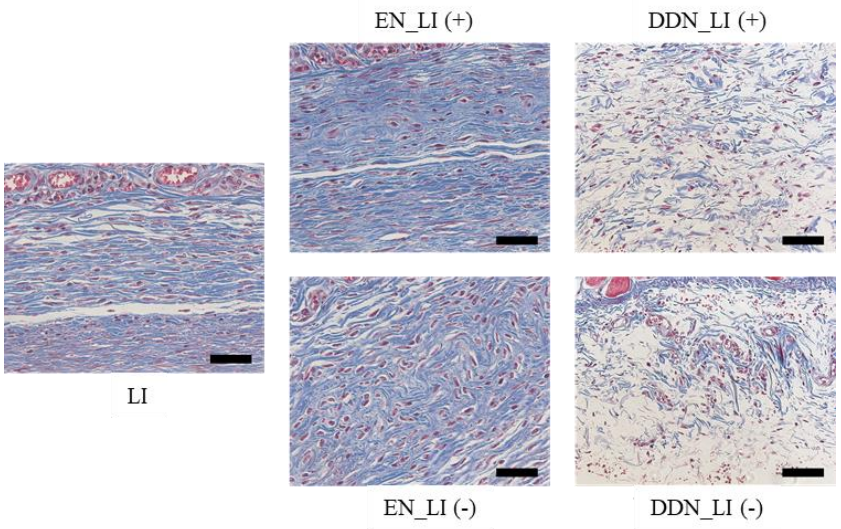

(b)

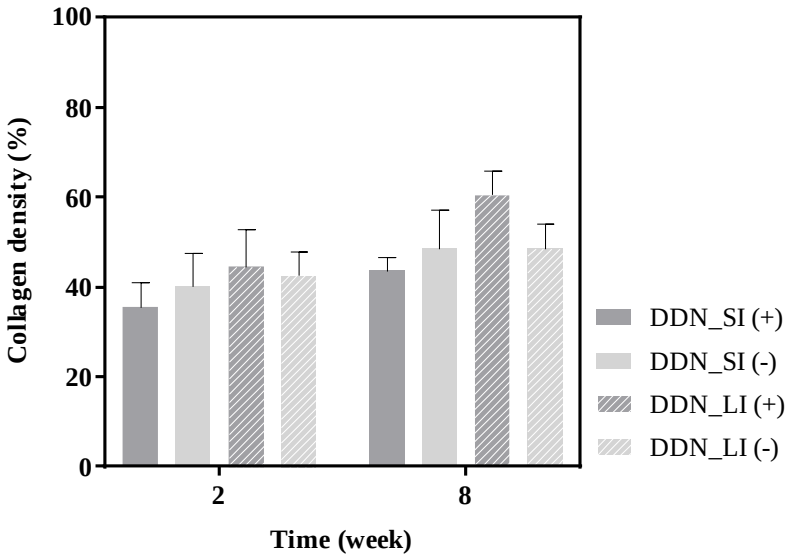

(c)

Figure 3.6. The collagen density around the silicone implants. Representative histological images of (a) SI and (b) LI groups obtained at 2 weeks after implantation. (c) show the comparison of DDN_SI and DDN_LI. The black arrows signify capsule thickness and the scale bars are 100 μm.

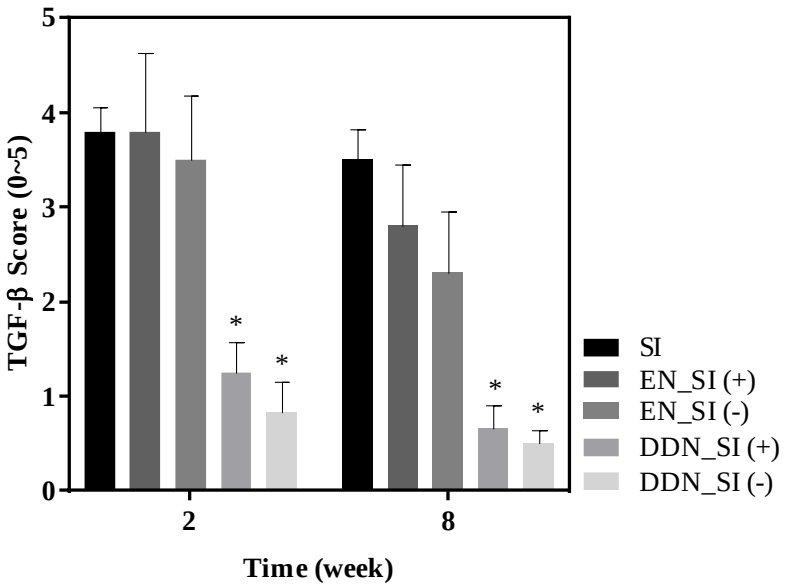
TGF-β Score (0~5)
0
1
2
3
4
5
*
*
*
*
2
8
Time (week)
SI
EN_SI (+)
EN_SI (-)
DDN_SI (+)
DDN_SI (-)

(a1)

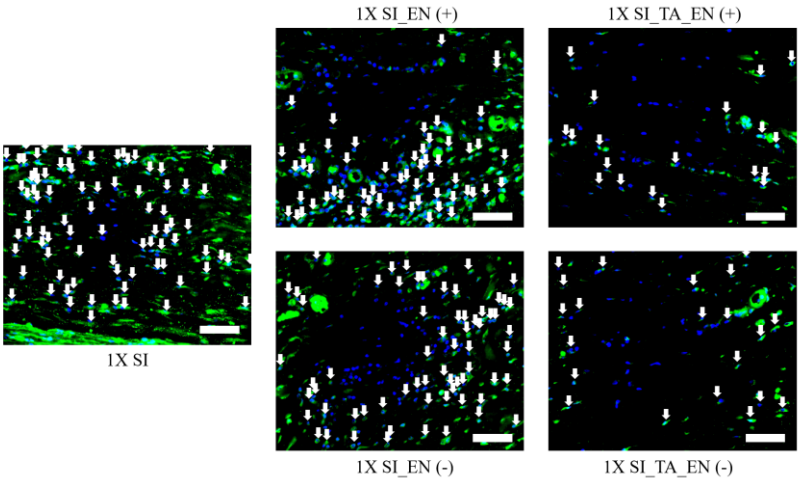
1X SI_EN (+)
1X SI_TA_EN (+)
1X SI
1X SI_EN (-)
1X SI_TA_EN (-)

(a2)

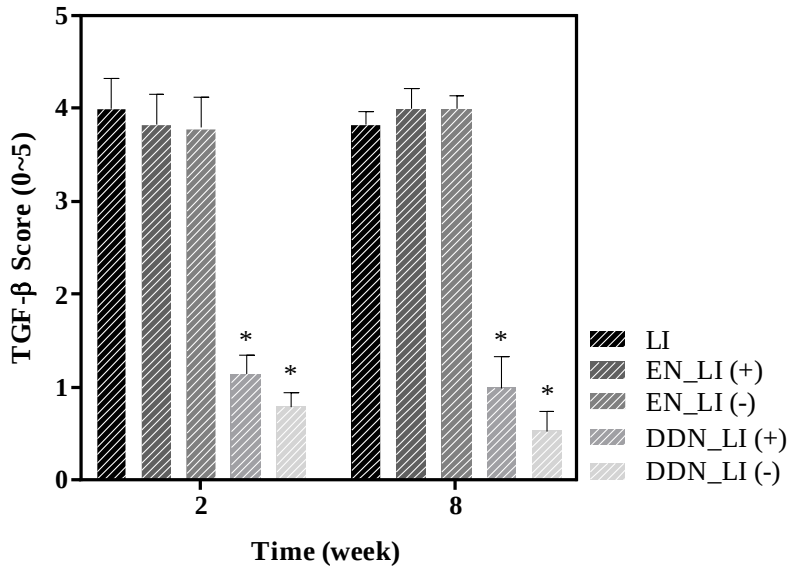
TGF-β Score (0~5)
5
4
3
2
1
0
2
8
Time (week)
*
*
*
*
LI
EN_LI (+)
EN_LI (-)
DDN_LI (+)
DDN_LI (-)

(b1)

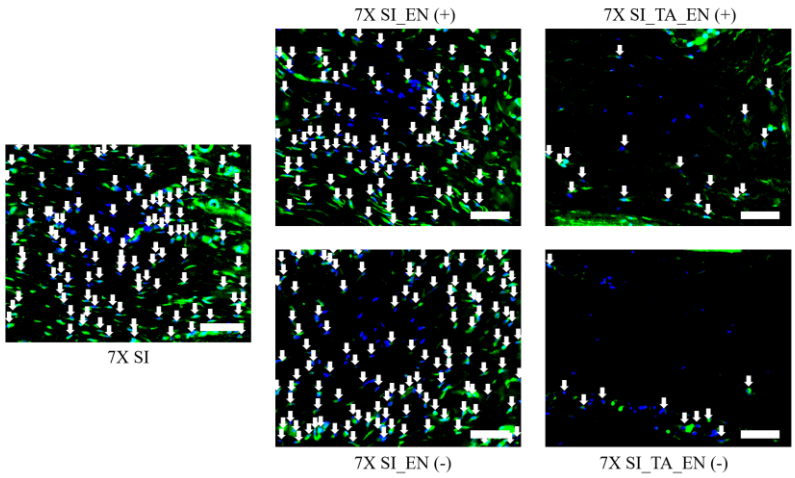
7X SI
7X SI_EN (+)
7X SI_TA_EN (+)
7X SI_EN (-)
7X SI_TA_EN (-)

(b2)

Figure 3.7. Profiles of TGF-ß expression in the tissues around the silicone implant samples of (a1) small and (b1) large sizes. Asterisk (*) represents a statistically significant difference compared with the intact SI and LI, respectively ($P < 0.01$). Representative IF-stained images of the tissues around the silicone implant samples of (a2) small and (b2) large sizes obtained at 8 weeks after implantation. White arrow heads indicate the locations of the cells with a double positive signal of green and blue. Scale bars are 100 μm.

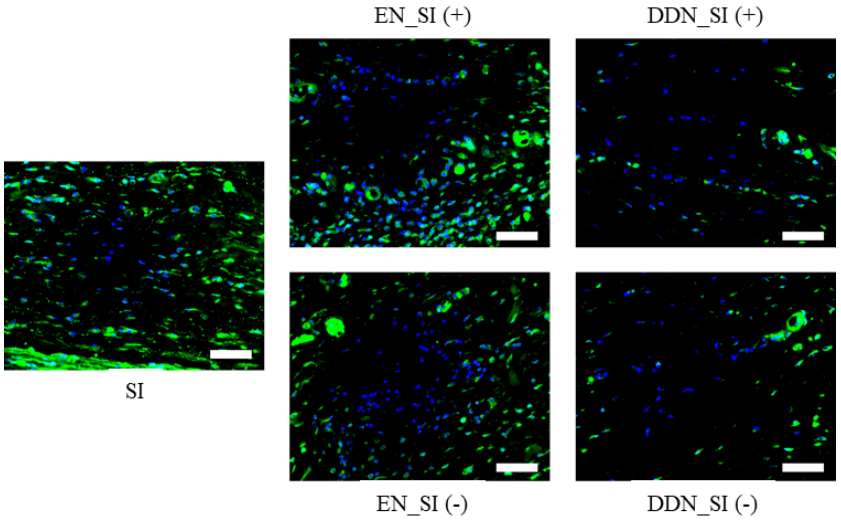

(a)

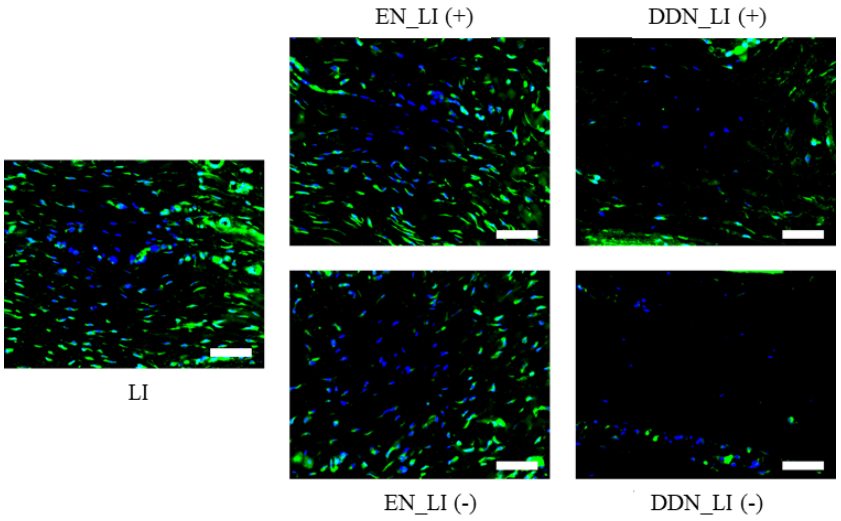

(b)

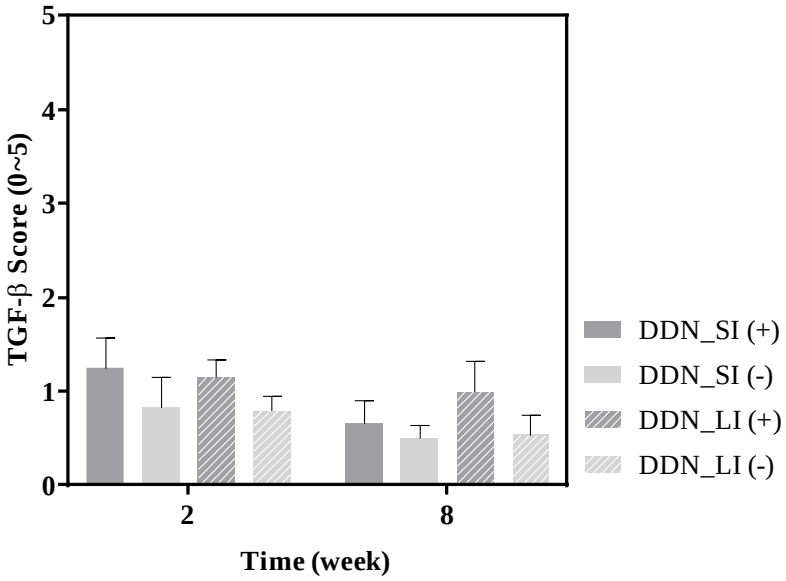

(c)

Figure 3.8. The TGF−β expression in the capsule tissue around the silicone implants. Representative histological images of (a) SI and (b) LI groups obtained at 8 weeks after implantation. (c) show the comparison of DDN_SI and DDN_LI. The scale bars are 100 μm.

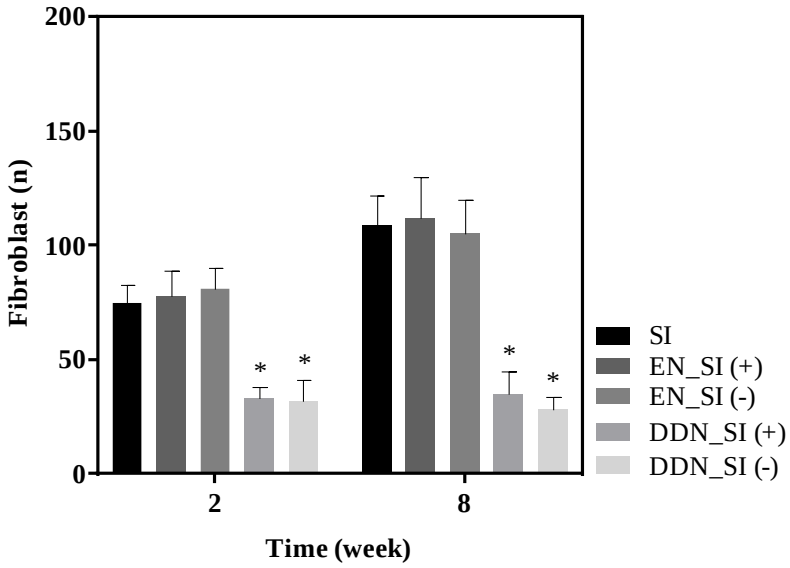
200
150
100
50
0
Fibroblast (n)
*
*
*
*
2
8
Time (week)
SI
EN_SI (+)
EN_SI (-)
DDN_SI (+)
DDN_SI (-)

(a1)

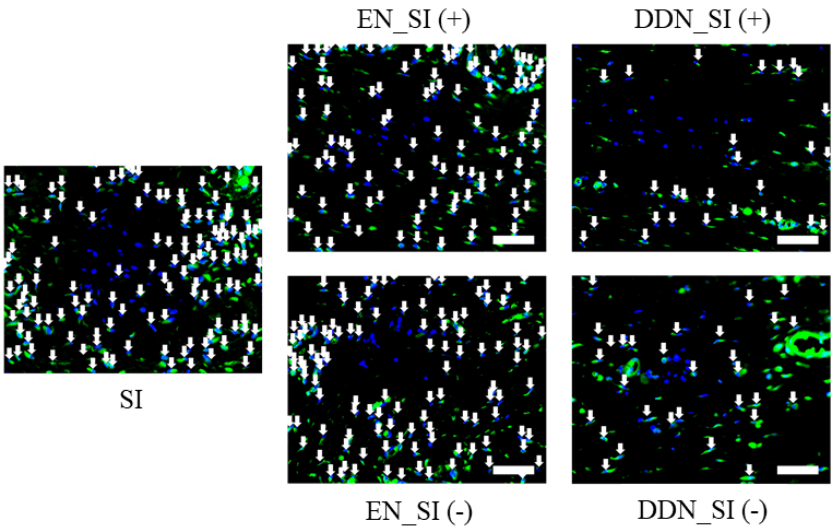
EN_SI (+)
DDN_SI (+)
SI
EN_SI (-)
DDN_SI (-)

(a2)

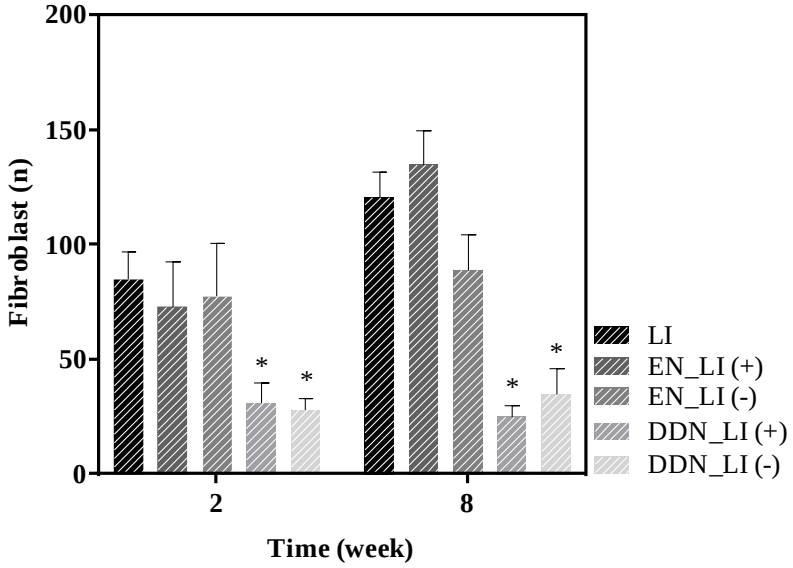
200
150
100
50
0
Fibroblast (n)
*
*
*
*
2
8
Time (week)
LI
EN_LI (+)
EN_LI (-)
DDN_LI (+)
DDN_LI (-)

(b1)

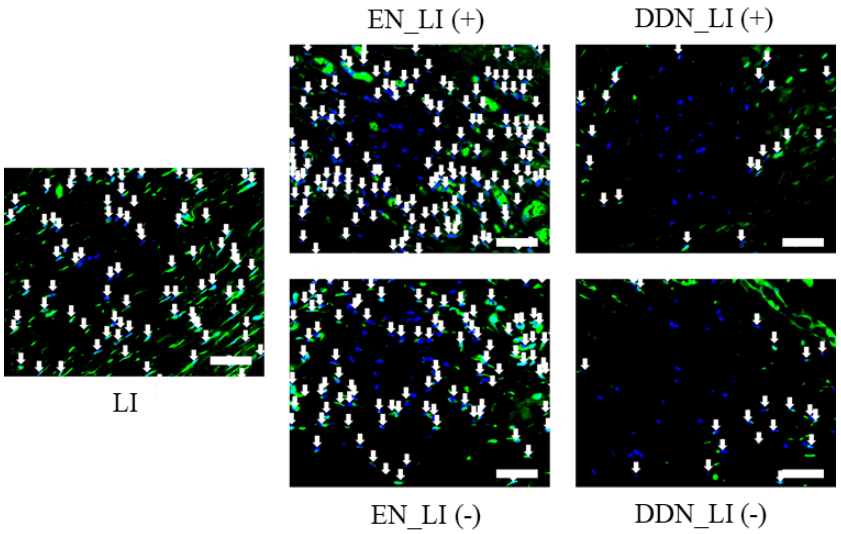
EN_LI (+)
DDN_LI (+)
LI
EN_LI (-)
DDN_LI (-)

(b2)

Figure. 3.9. Profiles of fibroblast number in the tissues around the silicone implant samples of (a1) small and (b1) large sizes. Asterisk (*) represents a statistically significant difference compared with the intact SI and LI, respectively ($P < 0.01$). Representative IF-stained images of the tissues around the silicone implant samples of (a2) small and (b2) large sizes obtained at 8 weeks after implantation. White arrow heads indicate the locations of the cells with a double positive signal of green and blue. Scale bars are 100 μm.

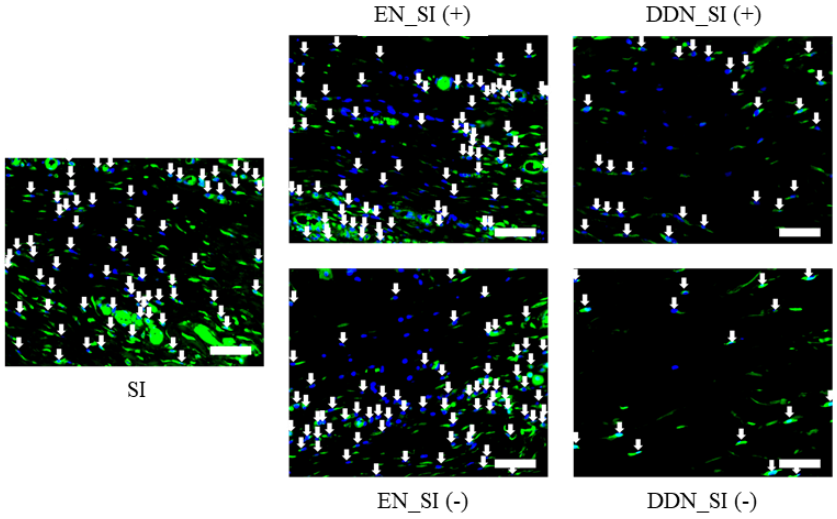

(a)

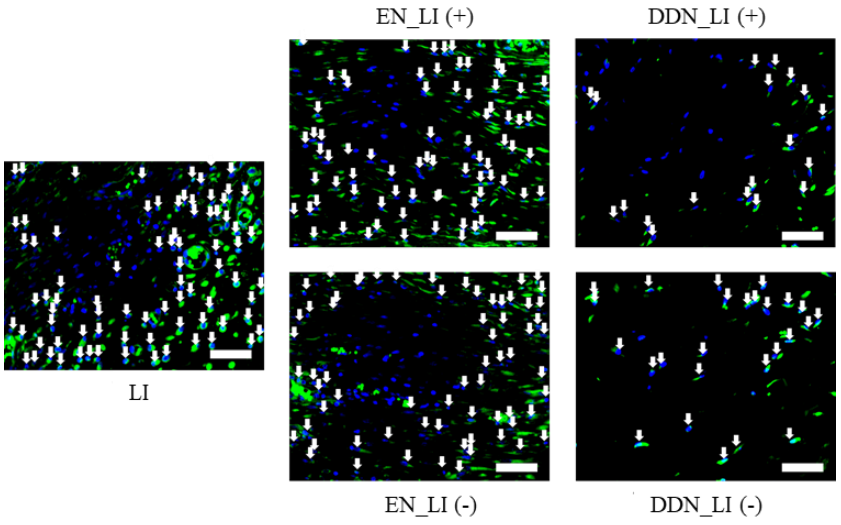

(b)

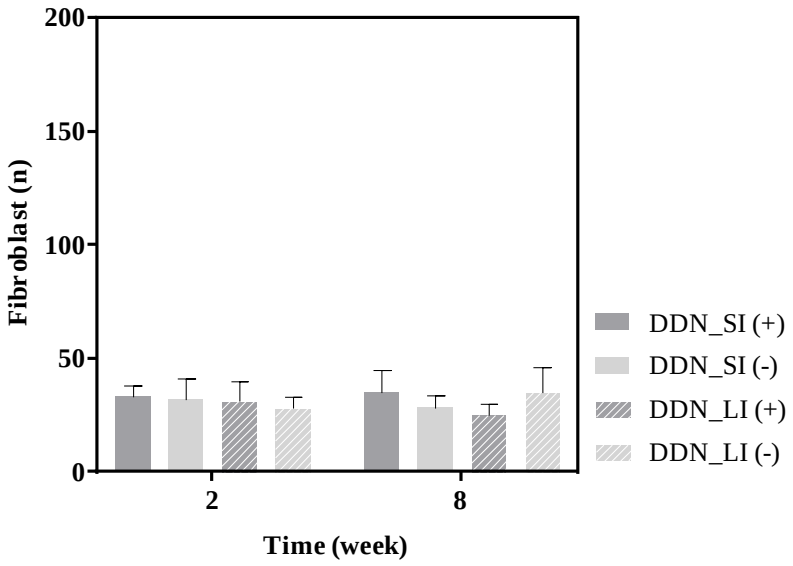

(c)

Figure 3.10. The fibroblast number in the capsule tissue around the silicone implants. Representative histological images of (a) SI and (b) LI groups obtained at 2 weeks after implantation. (c) show the comparison of DDN_SI and DDN_LI. The white arrows signify double signaling of fibroblast and the scale bars are 100 μm.

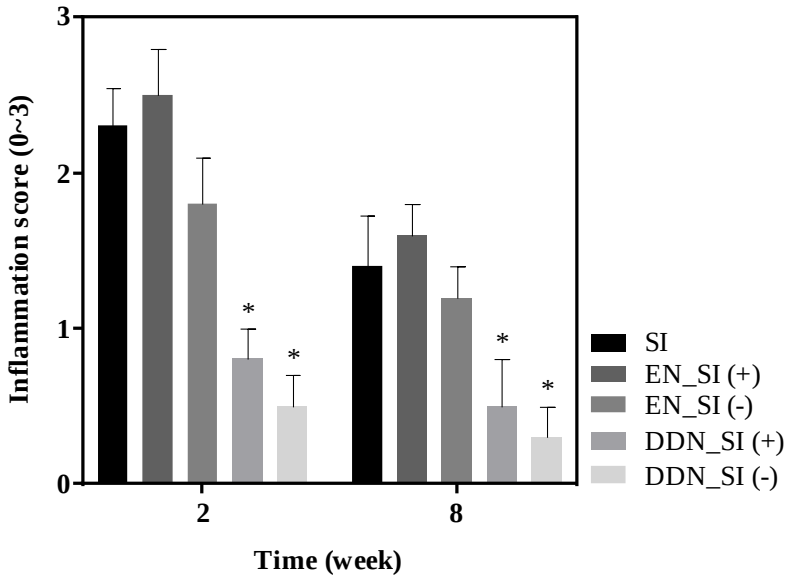
Inflammation score (0~3)
3
2
1
0
*
*
*
*
2
8
Time (week)
SI
EN_SI (+)
EN_SI (-)
DDN_SI (+)
DDN_SI (-)

(a1)

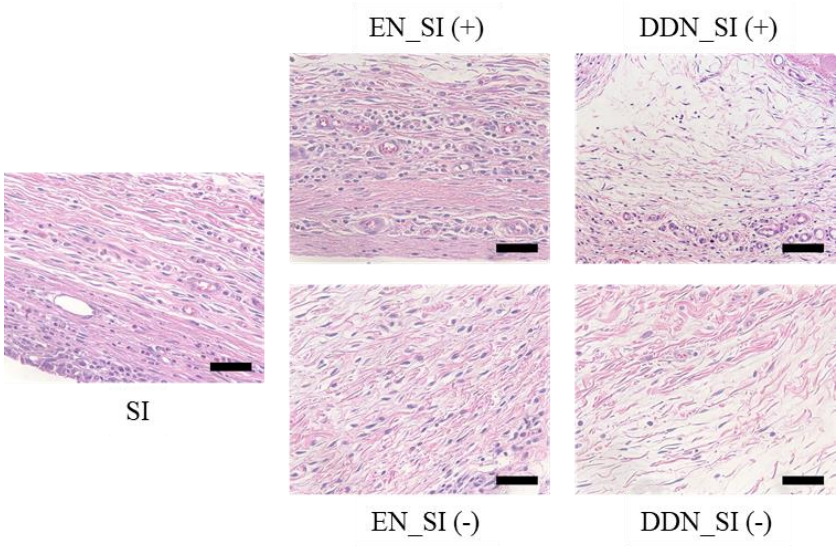
EN_SI (+)
DDN_SI (+)
SI
EN_SI (-)
DDN_SI (-)

(a2)

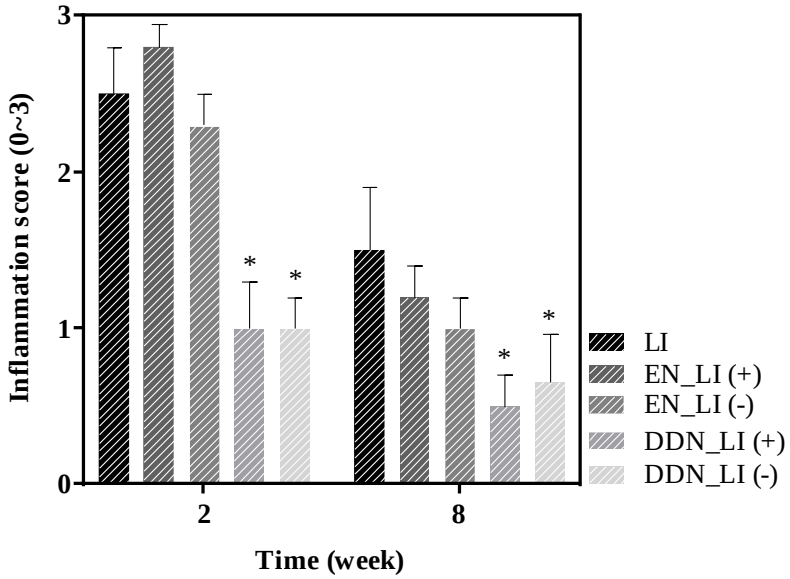
Inflammation score (0~3)
3
2
1
0
2
8
Time (week)
*
*
*
*
LI
EN_LI (+)
EN_LI (-)
DDN_LI (+)
DDN_LI (-)

(b1)

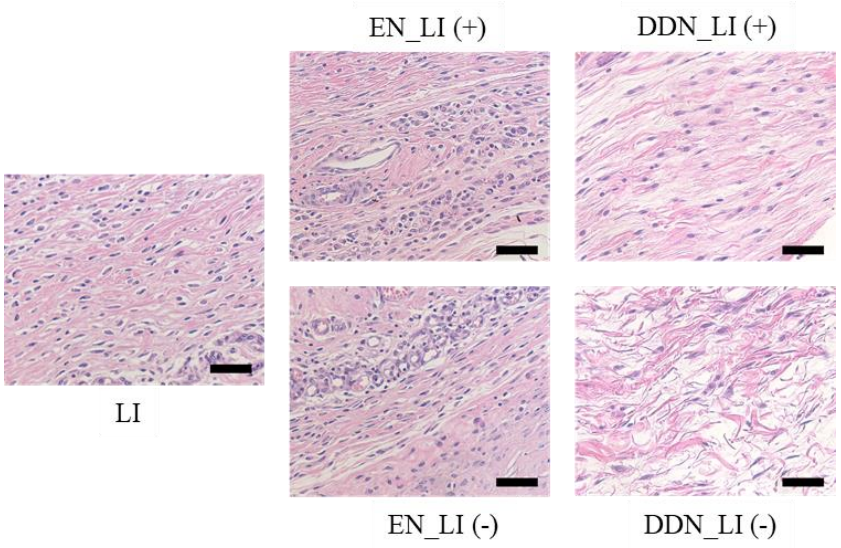
EN_LI (+)
DDN_LI (+)
LI
EN_LI (-)
DDN_LI (-)

(b2)

Figure 3.11. Profiles of inflammation degree around the silicone implant samples of (a1) small and (b1) large sizes. Asterisk (*) represents a statistically significant difference compared with the intact SI and LI, respectively ($P < 0.01$). Representative H&E-stained images of the tissues around the silicone implant samples of (a2) small and (b2) large sizes obtained at 2 weeks after implantation. Scale bars are 100 μm.

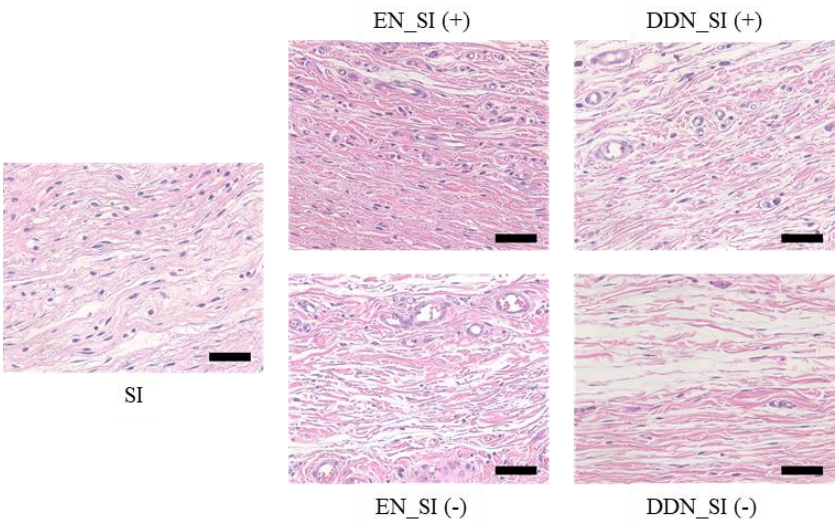

(a)

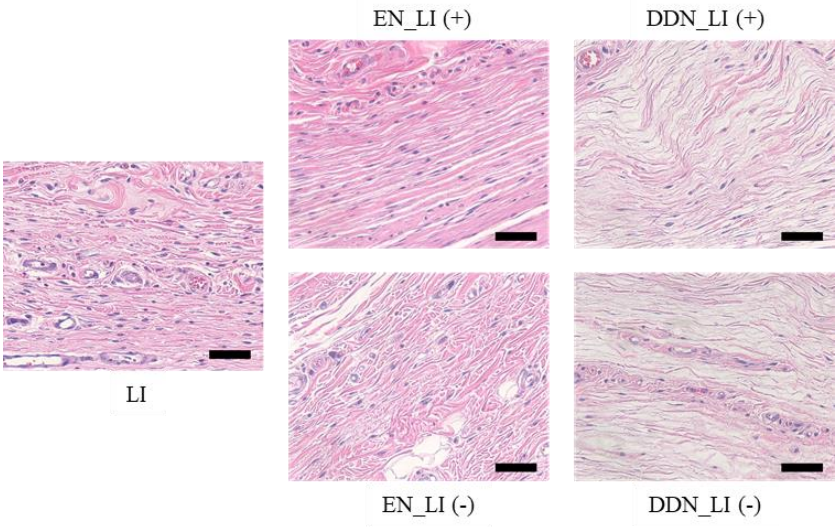

(b)

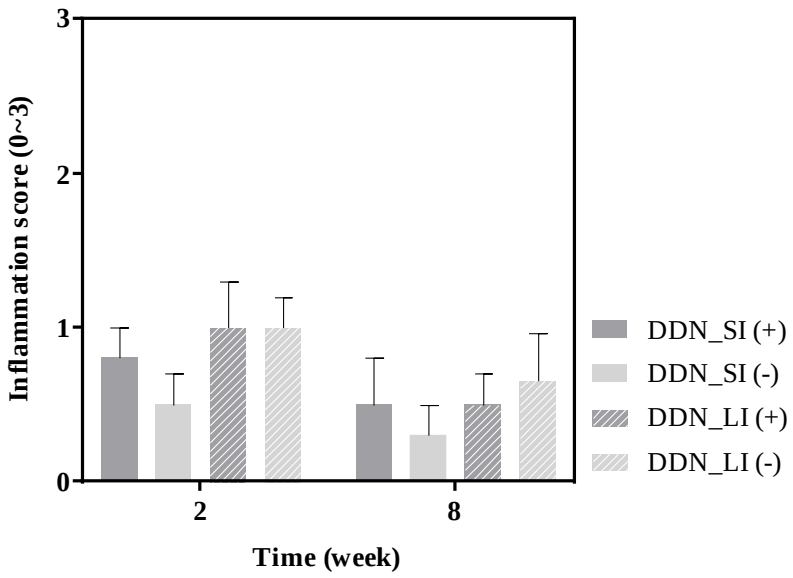

(c)

Figure 3.12. The degree of inflammation in the capsule tissue around the silicone implants. Representative histological images of (a) SI and (b) LI groups obtained at 8 weeks after implantation. (c) show the comparison of DDN_SI and DDN_LI. The scale bars are 100 μm.

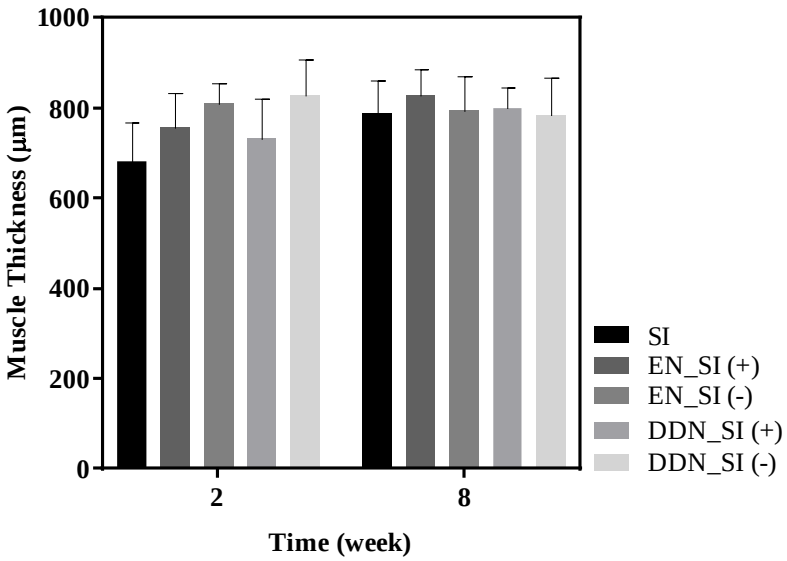
1000
800
600
400
200
0
Muscle Thickness (μm)
2
8
Time (week)
SI
EN_SI (+)
EN_SI (-)
DDN_SI (+)
DDN_SI (-)

(a1)

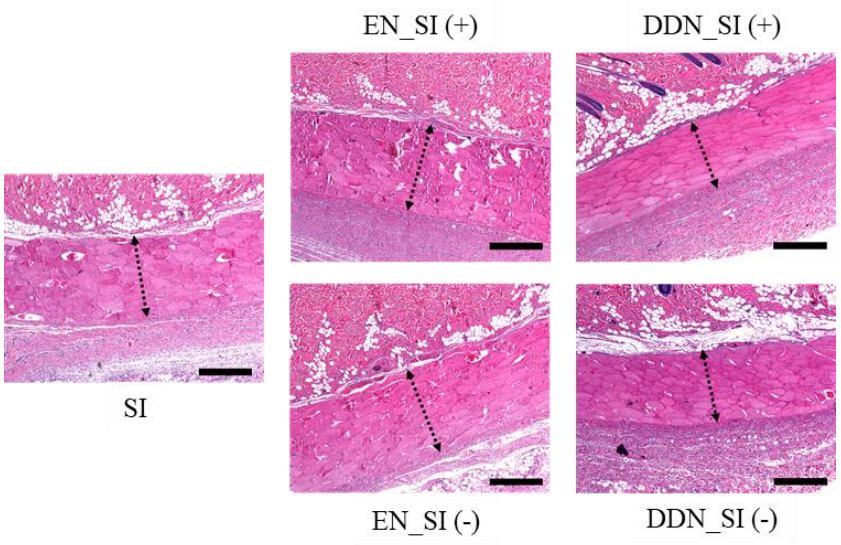
EN_SI (+)
DDN_SI (+)
SI
EN_SI (-)
DDN_SI (-)

(a2)

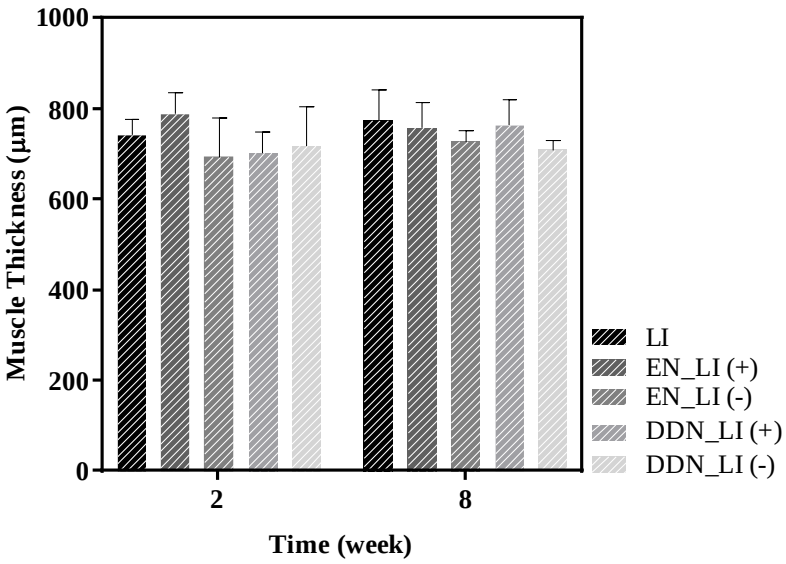
1000
800
600
400
200
0
Muscle Thickness (μm)
2
8
Time (week)
LI
EN_LI (+)
EN_LI (-)
DDN_LI (+)
DDN_LI (-)

(b1)

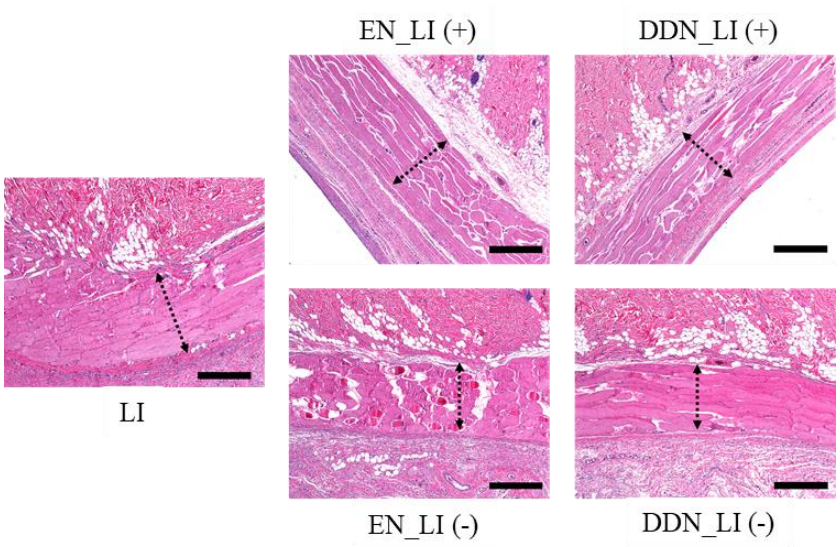
EN_LI (+)
DDN_LI (+)
LI
EN_LI (-)
DDN_LI (-)

(b2)

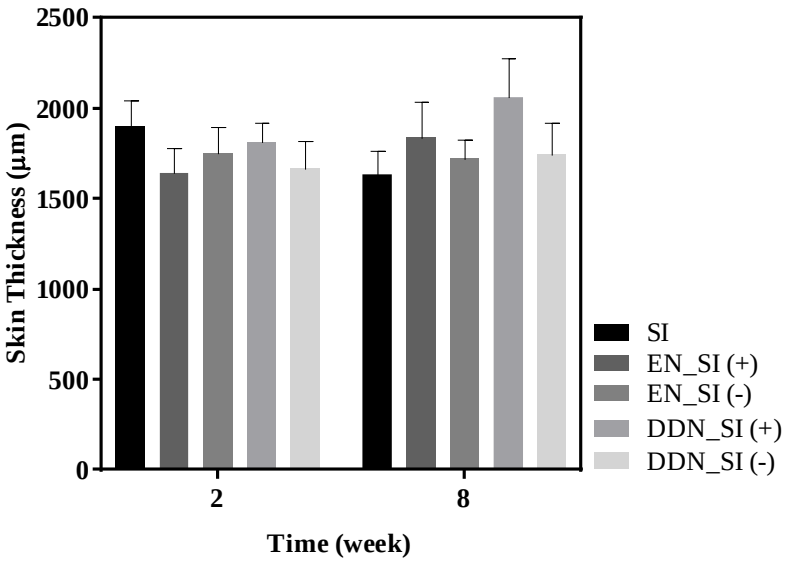
2500
2000
1500
1000
500
0
Skin Thickness (μm)
2
8
Time (week)
SI
EN_SI (+)
EN_SI (-)
DDN_SI (+)
DDN_SI (-)

(c1)

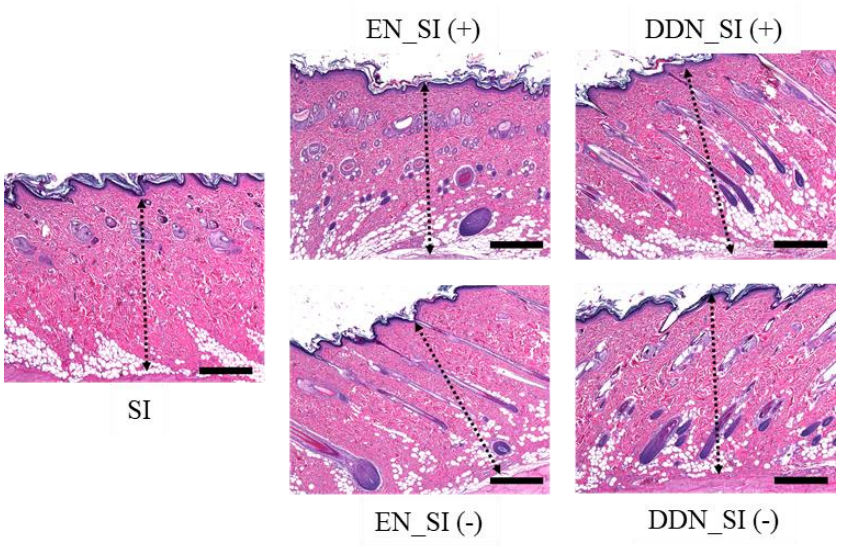
EN_SI (+)
DDN_SI (+)
SI
EN_SI (-)
DDN_SI (-)

(c2)

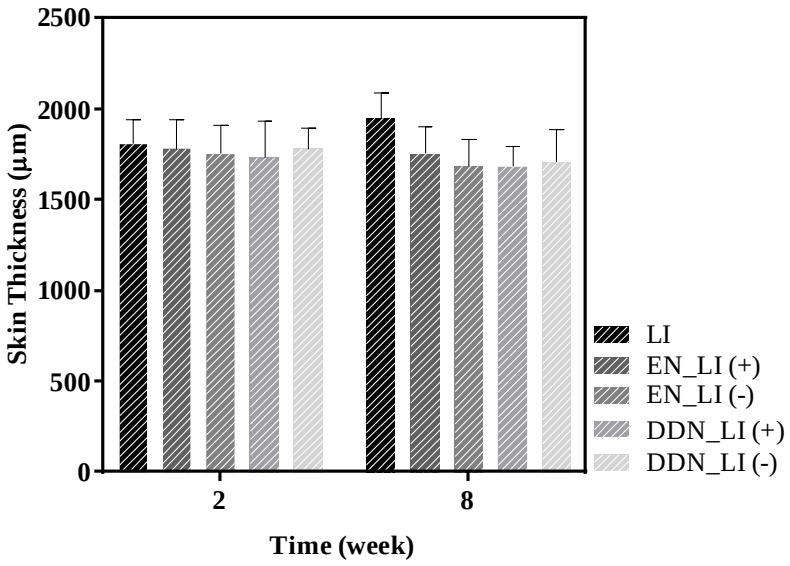
2500
2000
1500
1000
500
0
Skin Thickness (μm)
2
8
Time (week)
LI
EN_LI (+)
EN_LI (-)
DDN_LI (+)
DDN_LI (-)

(d1)

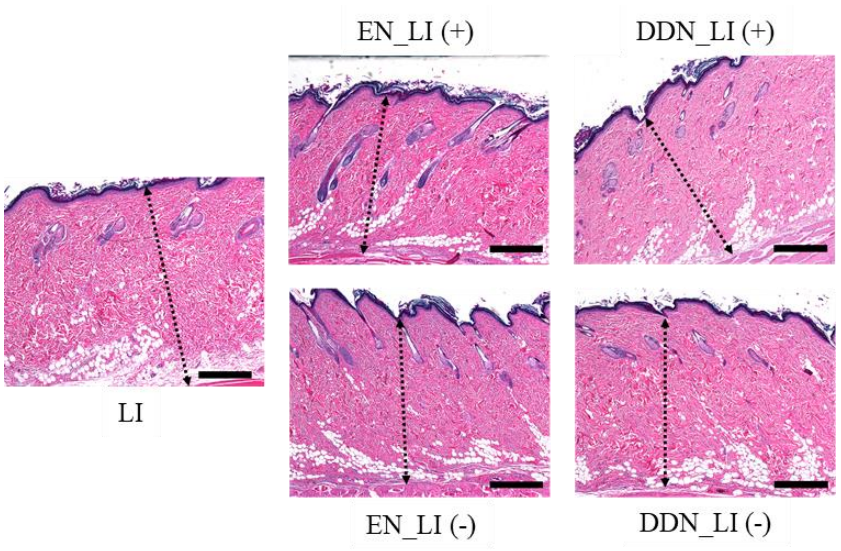
EN_LI (+)
DDN_LI (+)
LI
EN_LI (-)
DDN_LI (-)

(d2)

Figure 3.13. Side effect evaluation of the silicone implant samples. Profiles of muscle thickness around the silicone implant samples of (a1) small and (b1) large sizes. Asterisk (*) represents a statistically significant difference compared with the intact SI and LI, respectively ($P < 0.01$). Representative H&E-stained images used for muscle thickness evaluation around the silicone implant samples of (a2) small and (b2) large sizes obtained at 8 weeks after implantation. Black arrows indicate the muscle thickness. Scale bars are 500 μm. Profiles of skin thickness around the silicone implant samples of (c1) small and (d1) large sizes. Asterisk (*) represents a statistically significant difference compared with the intact SI and LI, respectively ($P < 0.01$). Representative H&E-stained images used for skin thickness evaluation around the silicone implant samples of (c2) small and (d2) large sizes obtained at 8 weeks after implantation. Black arrows indicate the skin thickness. Scale bars are 500 μm.

3.4 Discussion

Fibrotic capsule formation is a major complication of silicone implants and is caused mainly by upregulated and prolonged inflammation after implant insertion (4, 80, 83). Therefore, the local, sustained delivery of an anti-inflammatory drug, such as triamcinolone, around silicone implants could be beneficial by modulating inflammation and ultimately suppressing fibrosis (103). However, silicone implants are produced in various sizes to meet the needs of patients and specific purposes (88, 104). Thus, from a practical perspective, it would not be easy to develop a manufacturing procedure to prepare a coating with reproducible drug loading and delivery profiles applicable for all available implant sizes. Silicone implants for breast augmentation and reconstruction are generally produced in various sizes, with the largest implant being approximately 6 – 7 times larger than the smallest (91, 92).

Therefore, I suggest a net made of biocompatible, elastic polyurethane for the local, sustained delivery of triamcinolone around silicone implants of various sizes. The drug-loaded elastic net, i.e., the DDN herein, was prepared as a prototype, which could just wrap the small silicone implant sample (i.e., the SI sample) without strain. My results reveal that the same DDN could also wrap the implant sample 7 times larger in size (i.e., the LI sample) with a strain of 72%

due to the elastic property of polyurethane (Figures 3.1c, d). Importantly, the strain needed to wrap the LI sample was much lower than the strain at break (260 – 280%) of the DDN used in this work.

Under this condition, each of the nanofibers appeared to not be under much strain due to their arrangement in random directions (Figures 3.1a–d), and possibly because of this, the drug release profiles did not vary between the unstrained and strained DDNs (Figure 3.3). Therefore, when implanted in living animals, an antifibrotic effect of triamcinolone was evident around both the large and small implant samples wrapped with the same DDN, which was similarly effective across the entire surface of the implant (Figures 3.4–13).

My *in vivo* results also showed that the DDN did not exhibit the side effects of triamcinolone, such as muscle and skin thinning, around the wrapped implant samples (Figure 3.13). The triamcinolone dose for the strand was selected to be 1.38 ± 0.07 μg/cm; thus, the total dose for the DDN was 25.16 ± 1.23 μg, considering the total length of the drug–loaded strand used to prepare a single DDN (18.28 cm). Therefore, the drug dose per unit surface area of the implant sample could be calibrated to 3.19 and 1.08 μg/cm^2, given the total surface area of 7.88 and 23.32 cm^2 for the SI and LI samples, respectively. These doses of triamcinolone are within the range reported in my previous work (30), in which fibrosis was effectively

suppressed without causing side effects.

In addition to silicone implants, there are many different implantable medical devices available for clinical use, and their implantation often involves a relatively large wound. Therefore, postimplantation complications, such as pain, infection or impaired wound healing, can occur (76, 105). To resolve such a specific issue, the DDN could also be applied for the local, sustained release of other drugs of interest around an implanted device (106–108). More importantly, the DDN could be produced in a single size standardized for each category of implantable medical device, such as orthopedic fixation devices, electronic devices (e.g., pacemakers, deep brain stimulators) or drug infusion pumps (109–116). Thus, DDNs of a single size can be applied around the surface of medical devices of various sizes simply through a postprocess during manufacturing and still effectively modulate inflammation, prevent infection or even facilitate wound repair around the implanted device.

3.5 Conclusion

I propose a drug-loaded net made of an elastic, biocompatible polymer to wrap silicone implants produced in various sizes. The DDN can be made with electrospun, randomly oriented polyurethane nanofibers and thus be stretched to cover an implant 7 times larger in size without noticeable defects or changes in the drug release profile. When wrapped with the same DDN, therefore, all silicone implants in this size range can suppress fibrosis with similar efficacy due to the reproducible, local, sustained release of triamcinolone. Triamcinolone released from the strands of the DDN can also diffuse to cover the entire surface of the implant, resulting in a similar antifibrotic effect on both tissues in direct contact with the DDN and bare silicone. Therefore, I conclude that an elastic DDN loaded with triamcinolone has the potential to prevent fibrosis around silicone implants manufactured in various sizes.

Chapter 4

Conclusion and Perspectives

Recent years have witnessed a rapid growth of the medical device market. In order to meet diverse patients' demands, numerous devices have been developed. Each device has its own purpose and use, including, for instance, tissue connection and replacement of the human breast. However, the use of such medical devices may cause some unexpected side effects, such as

inflammation, which leads to pain, large scars, abnormal fibrosis, and capsular contractures, to the effect of requiring an additional surgery. To overcome these side effects, various drug delivery systems—most commonly, oral drug administration and local injection—have been developed and used in clinical practice.

However, conventional administration routes have limitations, such as low drug bioavailability, hepatoxicity, and aichmophobia (fear of needle) in patients. In the present dissertation, I developed a strand-based drug delivery carrier that has many advantages, such as providing full control of the drug delivery function and individual flexibility or rigidity. Since I developed the individual drug delivery carrier based on the strand, it is compatible with many medical devices such as surgical suture, silicone implant and, therefore, does not require any changes or modifications of current functions and modes of usage of medical devices.

More specifically, I physically braided the strands on surgical sutures so as to create a local drug delivery system. Therefore, through controlling the drug delivery profile, the manufactured strand can reduce inflammation and pain without compromising on the mechanical strength of suture.

Secondly, I developed an individual drug delivery elastic net to cover flexible silicone implants so as to reduce inflammation around the wound site. According to recent estimates, more than 30% of

patients suffer from abnormal fibrosis caused by inflammation, which can eventually lead to the formation of capsular contractures, bringing pain and potentially necessitating a second surgery. Furthermore, considering that patients' body sizes can vary considerably, an effective drug delivery system for various sizes of silicone implants is necessary. However, creating such system is difficult, and silicone implants may require additional procedures to reduce inflammation. In the present study, I managed to create the drug delivery elastic net that can not only cover the entire range of different sizes of silicone implants, but also deliver drugs up to 4 weeks of the acute inflammatory period. Through *in vivo* experiments, I demonstrated that stretched or non-stretched elastic net groups had similar drug release patterns and anti-inflammatory effects. These results suggest, regardless of that whether the strand was stretched or not, it did not alter or destroy the nano-fibrous structure and, therefore, successfully sustained the drug release profile.

The results of my experiments showed that individual strands can function as a controllable drug delivery system on medical devices without changing the functions of the latter. Therefore, the manufactured system has a great potential in terms of its further applications in the medical field. For instance, various drugs can be loaded to electrospun or electrosprayed sheet which can easily control the drug release profiles (98, 117-121). These approach can

apply to my developed strand where can be used in other medical devices. And, the use of the fabricated strand-based carrier can expand to other medical devices beyond sutures and silicone implants I tested in the present study. Specifically, the manufactured strands can be attached to the surface of an implantable medical device and elongate up to 250% of its original size. Moreover, the strand-based carrier can deliver the drug directly to the local site within the therapeutic window. Furthermore, it also requires a smaller amount of drugs as compared the oral administration or injection approaches. In summary, the developed strand-based controllable drug delivery system can effectively deliver anti-inflammatory drugs and successfully fits various sizes of implantable medical devices.

Reference

1. Maisel WH. Medical device regulation: an introduction for the practicing physician. Ann Intern Med. 2004;140(4):296-302.
2. Khan W, Muntimadugu E, Jaffe M, Domb AJ. Implantable medical devices. Focal controlled drug delivery: Springer; 2014. p. 33-59.
3. Anderson JM. Biological responses to materials. Annu Rev Mater Res 2001;31(1):81-110.
4. Tang L, Eaton JW. Inflammatory responses to biomaterials. Am J Clin Pathol. 1995;103(4):466-471.
5. Onuki Y, Bhardwaj U, Papadimitrakopoulos F, Burgess DJ. A review of the biocompatibility of implantable devices: current challenges to overcome foreign body response. SAGE Publications; 2008; 2(6):1003-1015.
6. Rolfe B, Mooney J, Zhang B, Jahnke S, Le S-J, Chau Y-Q, et al. The fibrotic response to implanted biomaterials: implications for tissue engineering. Regenerative Medicine and Tissue Engineering-Cells and Biomaterials: InTech; 2011.
7. Kim BH, Park M, Park HJ, Lee SH, Choi SY, Park CG, et al. Prolonged, acute suppression of cysteinyl leukotriene to reduce capsular contracture around silicone implants. Acta Biomater. 2017;51:209-219.
8. Lambert JD, Kennett MJ, Sang S, Reuhl KR, Ju J, Yang CS. Hepatotoxicity of high oral dose (−)-epigallocatechin-3-gallate in mice. Food Chem Toxicol. 2010;48(1):409-416.
9. Huh BK, Kim BH, Kim S-N, Park CG, Lee SH, Kim KR, et al. Surgical suture braided with a diclofenac-loaded strand of poly (lactic-co-glycolic acid) for local, sustained pain mitigation. Mater Sci Eng C. 2017;79:209-215.
10. Morais JM, Papadimitrakopoulos F, Burgess DJ. Biomaterials/tissue interactions: possible solutions to overcome foreign body response. The AAPS journal. 2010;12(2):188-196.
11. Ming X, Nichols M, Rothenburger S. In vivo antibacterial efficacy of MONOCRYL plus antibacterial suture (Poliglecaprone 25 with triclosan). Surg Infect (Larchmt). 2007;8(2):209-214.
12. Obermeier A, Schneider J, Wehner S, Matl FD, Schieker M, von Eisenhart-Rothe R, et al. Novel high efficient coatings for anti-microbial surgical sutures using chlorhexidine in fatty acid slow-release carrier systems. PloS one. 2014;9(7):e101426.
13. Obermeier A, Schneider J, Föhr P, Wehner S, Kühn K-D, Stemberger A, et al. In vitro evaluation of novel antimicrobial coatings for surgical sutures using octenidine. BMC microbiology. 2015;15(1):1-8.
14. Zurita R, Puiggalí J, Rodríguez-Galán A. Loading and Release of Ibuprofen in Multi-and Monofilament Surgical Sutures. Macromol Biosci. 2006;6(9):767-775.

15. Shanmugasundaram O, Gowda RM, Saravanan D. Drug release and antimicrobial studies on polylactic acid suture. International Journal of Biotechnology and Molecular Biology Research. 2011;2(5):80-89.
16. Choudhury AJ, Gogoi D, Chutia J, Kandimalla R, Kalita S, Kotoky J, et al. Controlled antibiotic-releasing Antheraea assama silk fibroin suture for infection prevention and fast wound healing. Surgery. 2016;159(2):539-547.
17. Ming X, Rothenburger S, Nichols MM. In vivo and in vitro antibacterial efficacy of PDS plus (polidioxanone with triclosan) suture. Surg Infect (Larchmt). 2008;9(4):451-457.
18. Storch ML, Rothenburger SJ, Jacinto G. Experimental efficacy study of coated VICRYL plus antibacterial suture in guinea pigs challenged with Staphylococcus aureus. Surg Infect (Larchmt). 2004;5(3):281-288.
19. Edmiston CE, Seabrook GR, Goheen MP, Krepel CJ, Johnson CP, Lewis BD, et al. Bacterial adherence to surgical sutures: can antibacterial-coated sutures reduce the risk of microbial contamination? J Am Coll Surg. 2006;203(4):481-489.
20. Rothenburger S, Spangler D, Bhende S, Burkley D. In vitro antimicrobial evaluation of Coated VICRYL* Plus Antibacterial Suture (coated polyglactin 910 with triclosan) using zone of inhibition assays. Surg Infect (Larchmt). 2002;3(S1):s79-s87.
21. Barbolt TA. Chemistry and safety of triclosan, and its use as an antimicrobial coating on Coated VICRYL* Plus Antibacterial Suture (coated polyglactin 910 suture with triclosan). Surg Infect (Larchmt). 2002;3(S1):s45-s53.
22. Rozzelle CJ, Leonardo J, Li V. Antimicrobial suture wound closure for cerebrospinal fluid shunt surgery: a prospective, double-blinded, randomized controlled trial. J Neurosurg Pediatr. 2008; 2(2):111-117.
23. Justinger C, Moussavian MR, Schlueter C, Kopp B, Kollmar O, Schilling MK. Antibiotic coating of abdominal closure sutures and wound infection. Surgery. 2009;145(3):330-334.
24. He CL, Huang ZM, Han XJ. Fabrication of drug-loaded electrospun aligned fibrous threads for suture applications. J Biomed Mater Res A. 2009;89(1):80-95.
25. Hu W, Huang Z-M, Liu X-Y. Development of braided drug-loaded nanofiber sutures. Nanotechnology. 2010;21(31):315104.
26. Wang L, Chen D, Sun J. Layer-by-layer deposition of polymeric microgel films on surgical sutures for loading and release of ibuprofen. Langmuir. 2009;25(14):7990-7994.
27. Lee D-H, Kwon T-Y, Kim K-H, Kwon S-T, Cho D-H, Jang SH, et al. Anti-inflammatory drug releasing absorbable surgical sutures using poly (lactic-co-glycolic acid) particle carriers. Polym Bull. 2014;71(8):1933-1946.
28. Padmakumar S, Joseph J, Neppalli MH, Mathew SE, Nair SV, Shankarappa SA, et al. Electrospun polymeric core–sheath yarns as drug

eluting surgical sutures. ACS Appl Mater Interfaces. 2016;8(11):6925-6934.
29. Marques M, Brown S, Correia-Sá I, Cordeiro MND, Rodrigues-Pereira P, Gonçalves-Rodrigues A, et al. The impact of triamcinolone acetonide in early breast capsule formation in a rabbit model. Aesthetic Plast Surg. 2012;36(4):986-994.
30. Jeon BS, Shin BH, Huh BK, Kim BH, Kim S-N, Ji HB, et al. Silicone implants capable of the local, controlled delivery of triamcinolone for the prevention of fibrosis with minimized drug side effects. J Ind Eng Chem. 2018;63:168-180.
31. Wu X, Kubilay NZ, Ren J, Allegranzi B, Bischoff P, Zayed B, et al. Antimicrobial-coated sutures to decrease surgical site infections: a systematic review and meta-analysis. Eur J Clin Microbiol Infect Dis. 2017;36(1):19-32.
32. Rømsing J, Møiniche S, Østergaard D, Dahl JB. Local infiltration with NSAIDs for postoperative analgesia: evidence for a peripheral analgesic action. Acta Anaesthesiol Scand. 2000;44(6):672-683.
33. Kokki H. Nonsteroidal anti-inflammatory drugs for postoperative pain. Pediatr Drugs. 2003;5(2):103-123.
34. Bjarnason I, Hayllar J, Macpherson AJ, Russell A. Side effects of nonsteroidal anti-inflammatory drugs on the small and large intestine in humans. Gastroenterology. 1993;104(6):1832-1847.
35. Polisson R. Nonsteroidal anti-inflammatory drugs: practical and theoretical considerations in their selection. Am J Med. 1996;100(2):31S-6S.
36. Strazielle N, Khuth ST, Ghersi-Egea J-F. Detoxification systems, passive and specific transport for drugs at the blood–CSF barrier in normal and pathological situations. Adv Drug Deliv Rev. 2004;56(12):1717-1740.
37. Benet LZ, Kroetz D, Sheiner L, Hardman J, Limbird L. Pharmacokinetics: the dynamics of drug absorption, distribution, metabolism, and elimination. Goodman and Gilman's the pharmacological basis of therapeutics. 1996:3-27.
38. Sostres C, Gargallo CJ, Arroyo MT, Lanas A. Adverse effects of non-steroidal anti-inflammatory drugs (NSAIDs, aspirin and coxibs) on upper gastrointestinal tract. Best Pract Res Clin Gastroenterol. 2010;24(2):121-32.
39. Laine L. Gastrointestinal effects of NSAIDs and coxibs. J Pain Symptom Manag. 2003;25(2):32-40.
40. Amass W, Amass A, Tighe B. A review of biodegradable polymers: uses, current developments in the synthesis and characterization of biodegradable polyesters, blends of biodegradable polymers and recent advances in biodegradation studies. Polym Int. 1998;47(2):89-144.
41. Martina M, Hutmacher DW. Biodegradable polymers applied in tissue engineering research: a review. Polym Int. 2007;56(2):145-157.
42. Holland SJ, Tighe BJ, Gould PL. Polymers for biodegradable medical devices. 1. The potential of polyesters as controlled macromolecular release systems. J Control Release. 1986;4(3):155-180.

43. Bayraktar O, Malay Ö, Özgarip Y, Batıgün A. Silk fibroin as a novel coating material for controlled release of theophylline. Eur J Pharm Biopharm. 2005;60(3):373-381.
44. Cleuvers M. Mixture toxicity of the anti-inflammatory drugs diclofenac, ibuprofen, naproxen, and acetylsalicylic acid. Ecotoxicol Environ Saf. 2004;59(3):309-315.
45. Funk CD. Prostaglandins and leukotrienes: advances in eicosanoid biology. Science. 2001;294(5548):1871-1875.
46. Kurumbail RG, Stevens AM, Gierse JK, McDonald JJ, Stegeman RA, Pak JY, et al. Structural basis for selective inhibition of cyclooxygenase-2 by anti-inflammatory agents. Nature. 1996;384(6610):644-648.
47. Rømsing J, Østergaard D, Senderovitz T, Drozdziewicz D, Sonne J, Ravn G. Pharmacokinetics of oral diclofenac and acetaminophen in children after surgery. Pediatr Anesth. 2001;11(2):205-213.
48. Korpela R, Olkkola K. Pharmacokinetics of intravenous diclofenac sodium in children. Eur J Clin Pharmacol. 1990;38(3):293-295.
49. Standardization IOf. International Standard ISO 10993-10991 Biological Evaluation of Medical Devices-Part 1: Evaluation and Testing Within a Risk Management Process. 2009.
50. Naleway SE, Lear W, Kruzic JJ, Maughan CB. Mechanical properties of suture materials in general and cutaneous surgery. J Biomed Mater Res B. 2015;103(4):735-742.
51. Sultana N, Arayne MS, Shafi N. In vitro interaction studies of diltiazem with NSAIDs using UV spectrophotometry and RP-HPLC techniques. Pak J Pham Sci. 2007;20:199-202.
52. Sultan M, Stecher G, Stöggl WM, Bakry R, Zaborski P, Huck C, et al. Sample Pretreatment and Determination of Non Steroidal Anti-Inflammatory Drugs (NSAIDs) in Pharmaceutical Formulations and Biological Samples (Blood, Plasma, Erythrocytes) by HPLC-UV-MS and μ-HPLC. Curr Med Chem. 2005;12:573-588.
53. Lee JE, Park S, Park M, Kim MH, Park CG, Lee SH, et al. Surgical suture assembled with polymeric drug-delivery sheet for sustained, local pain relief. Acta Biomater. 2013;9(9):8318-8327.
54. Gorska T, Majczyński H, Zmysłowski W. Overground locomotion in intact rats: contact electrode recording. Acta Neurobiol Exp. 1997;58(3):227-237.
55. McMullen R, Bauza E, Gondran C, Oberto G, Domloge N, Farra CD, et al. Image analysis to quantify histological and immunofluorescent staining of ex vivo skin and skin cell cultures. Int J Cosmet Sci. 2010;32(2):143-154.
56. Kujala S, Pajala A, Kallioinen M, Pramila A, Tuukkanen J, Ryhänen J. Biocompatibility and strength properties of nitinol shape memory alloy suture in rabbit tendon. Biomaterials. 2004;25(2):353-358.
57. Foley A, Halbert J, Hewitt T, Crotty M. Does hydrotherapy improve

strength and physical function in patients with osteoarthritis—a randomised controlled trial comparing a gym based and a hydrotherapy based strengthening programme. Ann Rheum Dis. 2003;62(12):1162-1167.
58. Li Y-P, Pei Y-Y, Zhang X-Y, Gu Z-H, Zhou Z-H, Yuan W-F, et al. PEGylated PLGA nanoparticles as protein carriers: synthesis, preparation and biodistribution in rats. J Control Release. 2001;71(2):203-211.
59. Stevanović M, Radulović A, Jordović B, Uskoković D. Poly (DL-lactide-co-glycolide) nanospheres for the sustained release of folic acid. J Biomed Nanotechnol. 2008;4(3):349-358.
60. Pal T, Paul S, Sa B. Polymethylmethacrylate coated alginate matrix microcapsules for controlled release of diclofenac sodium. Pharmacol Pharm. 2011;2(02):56.
61. Shivakumar H, Desai B, Deshmukh G. Design and optimization of diclofenac sodium controlled release solid dispersions by response surface methodology. Indian J Pharm Sci. 2008.
62. Shen X, Yu D, Zhu L, Branford-White C, White K, Chatterton NP. Electrospun diclofenac sodium loaded Eudragit® L 100-55 nanofibers for colon-targeted drug delivery. Int J Pharm. 2011;408(1):200-207.
63. Vega E, Gamisans F, Garcia M, Chauvet A, Lacoulonche F, Egea M. PLGA nanospheres for the ocular delivery of flurbiprofen: drug release and interactions. J Pharm Sci. 2008;97(12):5306-5317.
64. Pharmacopeia US. 467 - Residual Solvents - Chemical tests. 2007:(In USP30).
65. Food U, Administration D. Guidance for Industry and FDA Staff-Class II Special Controls Guidance Document: Surgical Sutures. US Department of Health and Human Services. 2003:6-13.
66. Miao P, Balachandran W, Xiao P. Formation of ceramic thin films using electrospray in cone-jet mode. IEEE T Ind Appl. 2002;38(1):50-56.
67. Sheu M-T, Chou H-L, Kao C-C, Liu C-H, Sokoloski TD. Dissolution of diclofenac sodium from matrix tablets. Int J Pharm. 1992;85(1-3):57-63.
68. Kocbek P, Baumgartner S, Kristl J. Preparation and evaluation of nanosuspensions for enhancing the dissolution of poorly soluble drugs. Int J Pharm. 2006;312(1):179-186.
69. Gan TJ. Diclofenac: an update on its mechanism of action and safety profile. Curr Med Res Opin. 2010;26(7):1715-1731.
70. Albornoz CR, Bach PB, Mehrara BJ, Disa JJ, Pusic AL, McCarthy CM, et al. A paradigm shift in US Breast reconstruction: increasing implant rates. Plast Reconstr Surg. 2013;131(1):15-23.
71. Spear SL, Parikh PM, Goldstein JA. History of breast implants and the food and drug administration. Clin Plast Surg. 2009;36(1):15-21.
72. Champaneria MC, Wong WW, Hill ME, Gupta SC. The evolution of breast reconstruction: a historical perspective. World J Surg. 2012;36(4):730-742.

73. Henriksen TF, Fryzek JP, Hölmich LR, McLaughlin JK, Kjøller K, Høyer AP, et al. Surgical intervention and capsular contracture after breast augmentation: a prospective study of risk factors. Ann Plast Surg. 2005;54(4):343-351.
74. Headon H, Kasem A, Mokbel K. Capsular contracture after breast augmentation: an update for clinical practice. Arch Plast Surg. 2015;42(5):532-543.
75. Handel N, Jensen JA, Black Q, Waisman JR, Silverstein MJ. The fate of breast implants: a critical analysis of complications and outcomes. Plast Reconstr Surg. 1995;96(7):1521-1533.
76. Gabriel SE, Woods JE, O'Fallon WM, Beard CM, Kurland LT, Melton LJ. Complications leading to surgery after breast implantation. N Engl J Med. 1997;336(10):677-682.
77. Handel N, Cordray T, Gutierrez J, Jensen JA. A long-term study of outcomes, complications, and patient satisfaction with breast implants. Plast Reconstr Surg. 2006;117(3):757-767.
78. Momoh AO, Ahmed R, Kelley BP, Aliu O, Kidwell KM, Kozlow JH, et al. A systematic review of complications of implant-based breast reconstruction with prereconstruction and postreconstruction radiotherapy. Ann Surg Oncol. 2014;21(1):118-124.
79. Anderson JM. Mechanisms of inflammation and infection with implanted devices. Cardiovasc Pathol. 1993;2(3):33-41.
80. Jones KS, Effects of biomaterial-induced inflammation on fibrosis and rejection. Semin Immunol. 2008; 20(2):130-136.
81. Wick G, Backovic A, Rabensteiner E, Plank N, Schwentner C, Sgonc R. The immunology of fibrosis: innate and adaptive responses. Trends Immunol. 2010;31(3):110-119.
82. Leask A, Abraham DJ. TGF-β signaling and the fibrotic response. FASEB J. 2004;18(7):816-827.
83. Mack M. Inflammation and fibrosis. Matrix Biol. 2017.
84. Darby IA, Hewitson TD. Fibroblast differentiation in wound healing and fibrosis. Int Rev Cytol. 2007;257:143-179.
85. Bastos EM, Neto MS, Alves MTS, Garcia ÉB, Santos RA, Heink T, et al. Histologic analysis of zafirlukast's effect on capsule formation around silicone implants. Aesthetic Plast Surg. 2007;31(5):559-565.
86. Jindal A, Puskas JE, McClain A, Nedic K, Luebbers MT, Baker Jr JR, et al. Encapsulation and release of Zafirlukast from electrospun polyisobutylene-based thermoplastic elastomeric fiber mat. Eur Polym J. 2018;98:254-261.
87. Park S, Park M, Kim BH, Lee JE, Park HJ, Lee SH, et al. Acute suppression of TGF-ß with local, sustained release of tranilast against the formation of fibrous capsules around silicone implants. J Control Release. 2015;200:125-137.

88. Hidalgo DA. Breast augmentation: choosing the optimal incision, implant, and pocket plane. Plast Reconstr Surg. 2000;105(6):2202-2216.
89. Tebbetts JB, Hammond DC. A system for breast implant selection based on patient tissue characteristics and implant-soft tissue dynamics. Plast Reconstr Surg. 2002;109(4):1396-1409.
90. Carroll LA, Hanasono MM, Mikulec AA, Kita M, Koch RJ. Triamcinolone stimulates bFGF production and inhibits TGF-β1 production by human dermal fibroblasts. Dermatol Surg. 2002;28(8):704-709.
91. Gabrick KS, Markov NP, Chouairi F, Wu R, Persing SM, Abraham P, et al. A Predictive Model for Determining Permanent Implant Size During 2-Stage Implant Breast Reconstruction. Plastic and Reconstructive Surgery Global Open. 2018;6(5): e1790.
92. Singh N, Picha GJ, Murphy DK. Natrelle silicone breast implant follow-up study: Demographics, lifestyle, and surgical characteristics of more than 50,000 augmentation subjects. Plast Reconstr Surg. 2016;137(1):70-81.
93. Kim SH, Moon J-H, Kim JH, Jeong SM, Lee S-H. Flexible, stretchable and implantable PDMS encapsulated cable for implantable medical device. Biomedical Engineering Letters. 2011;1(3):199.
94. Zeplin PH, Larena-Avellaneda A, Schmidt K. Surface modification of silicone breast implants by binding the antifibrotic drug halofuginone reduces capsular fibrosis. Plast Reconstr Surg. 2010;126(1):266-74.
95. Ruiz-de-Erenchun R, de las Herrerías JD, Hontanilla B. Use of the transforming growth factor-β1 inhibitor peptide in periprosthetic capsular fibrosis: experimental model with tetraglycerol dipalmitate. Plast Reconstr Surg. 2005;116(5):1370-8.
96. Watkins P. Designing with stretch fabrics. 2011.
97. García-Millán E, Quintáns-Carballo M, Otero-Espinar FJ. Solid-state characterization of triamcinolone acetonide nanosuspensiones by X-ray spectroscopy, ATR Fourier transforms infrared spectroscopy and differential scanning calorimetry analysis. Data in brief. 2017;15:133-7.
98. Amna T, Hassan MS, Yang J, Khil M-S, Song K-D, Oh J-D, et al. Virgin olive oil blended polyurethane micro/nanofibers ornamented with copper oxide nanocrystals for biomedical applications. International journal of nanomedicine. 2014;9:891.
99. Maity S, Sarkar A. 4 - Monitoring fibrous capsule formation. In: Narayan RJ, editor. Monitoring and Evaluation of Biomaterials and their Performance In Vivo: Woodhead Publishing; 2017. p. 69-80.
100. Schäcke H, Döcke W-D, Asadullah K. Mechanisms involved in the side effects of glucocorticoids. Pharmacol Ther. 2002;96(1):23-43.
101. Schoepe S, Schäcke H, May E, Asadullah K. Glucocorticoid therapy-induced skin atrophy. Exp Dermatol. 2006;15(6):406-20.
102. Schakman O, Kalista S, Barbé C, Loumaye A, Thissen J-P. Glucocorticoid-induced skeletal muscle atrophy. Int J Biochem Cell Biol.

2013;45(10):2163-72.
103. Bressler NM, Edwards AR, Beck RW, Flaxel CJ, Glassman AR, Ip MS, et al. Exploratory analysis of diabetic retinopathy progression through 3 years in a randomized clinical trial that compares intravitreal triamcinolone acetonide with focal/grid photocoagulation. 2009;127(12):1566-71.
104. Cárdenas-Camarena L, Encinas-Brambila J. Round gel breast implants or anatomic gel breast implants: which is the best choice? Aesthetic Plast Surg. 2009;33(5):743-51.
105. Von Eiff C, Jansen B, Kohnen W, Becker K. Infections associated with medical devices. Drugs. 2005;65(2):179-214.
106. Huynh TTN, Padois K, Sonvico F, Rossi A, Zani F, Pirot F, et al. Characterization of a polyurethane-based controlled release system for local delivery of chlorhexidine diacetate. Eur J Pharm Biopharm. 2010;74(2):255-64.
107. Chen Y, Wang R, Zhou J, Fan H, Shi B. On-demand drug delivery from temperature-responsive polyurethane membrane. React Funct Polym. 2011;71(4):525-535.
108. Sivak WN, Zhang J, Petoud S, Beckman EJ. Incorporation of ionic ligands accelerates drug release from LDI-glycerol polyurethanes. Acta Biomater. 2010;6(1):144-153.
109. Rahaman MN, Yao A, Bal BS, Garino JP, Ries MD. Ceramics for prosthetic hip and knee joint replacement. J Am Ceram Soc. 2007;90(7):1965-1988.
110. Holmes C. The lithium/iodine-polyvinylpyridine pacemaker battery-35 years of successful clinical use. ECS Trans. 2007;6(5):1-7.
111. Mallela VS, Ilankumaran V, Rao NS. Trends in cardiac pacemaker batteries. Indian Pacing Electrophysiol J. 2004;4(4):201-212.
112. Beurskens NE, Tjong FV, Knops RE. End-of-life Management of Leadless Cardiac Pacemaker Therapy. Arrhythmia Electrophysiol Rev. 2017;6(3):129-133.
113. Coffey RJ. Deep brain stimulation devices: a brief technical history and review. Artif Organs. 2009;33(3):208-220.
114. Butson CR, McIntyre CC. Role of electrode design on the volume of tissue activated during deep brain stimulation. J Neural Eng. 2005;3(1):1-8.
115. Kleiner LW, Wright JC, Wang Y. Evolution of implantable and insertable drug delivery systems. J Control Release. 2014;181:1-10.
116. Bhatia G, Lau ME, Koury KM, Gulur P. Intrathecal Drug Delivery (ITDD) systems for cancer pain. F1000Research. 2013;2.
117. Lu T, Jing X, Song X, Wang X. Doxorubicin-loaded ultrafine PEG-PLA fiber mats against hepatocarcinoma. J Appl Polym Sci. 2012;123(1):209-217.
118. Hong Y, Fujimoto K, Hashizume R, Guan J, Stankus JJ, Tobita K, et al. Generating elastic, biodegradable polyurethane/poly (lactide-co-glycolide) fibrous sheets with controlled antibiotic release via two-stream

electrospinning. Biomacromolecules. 2008;9(4):1200-1207.
119. Jiang H, Fang D, Hsiao B, Chu B, Chen W. Preparation and characterization of ibuprofen-loaded poly (lactide-co-glycolide)/poly (ethylene glycol)-g-chitosan electrospun membranes. J Biomater Sci Polym Ed. 2004;15(3):279-296.
120. Xu X, Chen X, Ma Pa, Wang X, Jing X. The release behavior of doxorubicin hydrochloride from medicated fibers prepared by emulsion-electrospinning. Eur J Pharm Biopharm. 2008;70(1):165-170.
121. Liu D, Liu S, Jing X, Li X, Li W, Huang Y. Necrosis of cervical carcinoma by dichloroacetate released from electrospun polylactide mats. Biomaterials. 2012;33(17):4362-4369.

Abstract in Korean

국문 초록

본 논문은 이식 가능한 의료기기의 기능을 지원할 수 있는 스트랜드(Strand) 기반 약물 전달 의료기기의 설계, 제작 및 평가에 초점을 맞추고 있다. 이식 후 스트랜드 기반 약물 전달 의료기기의 생체적합성을 유지시키기 위해, 전기 방사 및 전기 분사 방법을 사용하여 생체 고분자를 이용한 스트랜드를 준비했다.

최근 몇 년 동안, 인간과 다른 동물의 질병을 진단, 치료, 치료, 예방하기 위해 수많은 의료기기가 개발되었다. 그러나, 의료기기를 제조하는데 사용되는 재료는 신체에 이질적인 물질이며, 따라서 염증으로부터 구형구축뿐만 아니라 통증과 비정상적인 섬유증을 일으킬 수 있다. 이러한 문제를 해결하기 위해 흔히 사용되는 접근법에는 경구 약물 투여와 약물 주사가 있으나, 이 접근법은 간독성이나 추가 통증과 같은 2차 부작용을 일으킬 수 있다. 의료기기의 국소 약물 전달 시스템을 통하여 이러한 부작용이 감소된 최근 연구의 발전에도 불구하고, 제어 된 약물 전달의 어려움 또는 의료기기의 기능 저하와 같은 제한 사항이 여전히 남아 있다.

앞서 언급한 문제를 해결하기 위해, 본 연구에서는 스트랜드를 기반으로 개별 약물 전달 캐리어를 개발했다. 이 캐리어는 의료기기의 기능을 손상시키지 않고 적정량의 약물을 국소 부위에 방출한다.

첫 번째 실험에서는, 스트랜드 기반의 약물 제어 전달 시스템을

포함하는 새로운 의료기기를 개발하였다. 개발된 약물전달 스트랜드는 봉합사의 원래 기능을 유지하고 염증으로부터 발생하는 고통을 완화시킬 수 있다. 이 스트랜드는 전기분사 방법으로 제조된 시트를 너비가 1.5mm로 절단한 후 봉합사에 물리적으로 결합하였다. 그 결과로, 이 약물전달 스트랜드가 결합된 봉합사는 염증으로 인한 고통을 억제함과 동시에, 봉합사의 기계적 강도를 유지하고 10일동안 지속적으로 약을 방출할 수 있었다.

두 번째 실험에서 실리콘 보형물에 의한 염증을 줄이기 위한 목적으로, 나는 약물 제어 전달 시스템을 가지고 있는 탄성망을 제작했다. 이 탄성 망은 너비가 3mm인 4개의 스트랜드로 제작되었다. 이때 스트랜드들은 폴리우레탄과 스테로이드제의 혼합물을 전기방사하여 제작하였다. 실리콘 삽입으로 인한 염증이 비정상적인 섬유증을 유발할 수 있다는 것은 널리 알려져 있으며 구형구축으로 이어진다. 이 구형구축은 통증을 유발시킬 뿐만 아니라 추가 수술을 필요로 한다. 그러나, 두 번째 실험의 결과에서 보듯이, 제조된 탄성 망은 염증을 억제하고, 비정상적인 섬유증, 그리고 구형구축의 발달을 억제했다. 또한 탄성 소재 특성상 다양한 크기의 임플란트에 감싸는 것이 가능할 수 있었다.

이러한 스트랜드 기반의 약물 전달 캐리어는 약물의 제어전달이 가능하며 탄성과 같은 각각의 개별적인 특성을 갖는다. 이 스트랜드는 상용화 된 의료기기에 적용 할 수 있기 때문에, 의료기기 각각의 기능을 유지하면서 약물 전달 시스템의 부작용이나 한계를 해결할 수 있는 추가적인 기능을 가지고 있다. 이 스트랜드 기반의 약물 전달 캐리어들은 원래 의료기기의 완전한 기능을 유지하면서 약물을 정확하게 제어하고

전달할 수 있는 효과적인 의료기기임이 입증되었다.

키워드: 염증, 약물 제어 전달, 스트랜드, 바이오폴리머, 의료기기

Student Number: 2013-31001

Acknowledgement